Journal of COMPUTATIONAL CHEMISTRY

Chalcogen-mercury bond formation and disruption in model Rabenstein's reactions: a computational analysis

Journal:	*Journal of Computational Chemistry*
Manuscript ID	JCC-20-0185.R2
Wiley - Manuscript type:	Full Paper
Date Submitted by the Author:	n/a
Complete List of Authors:	Madabeni, Andrea; Università degli Studi di Padova, Scienze Chimiche DallaTiezza, Marco; Università degli Studi di Padova, Scienze Chimiche Nogara, Pablo; Universidade Federal de Santa Maria Folorunsho, Omage; Universidade Federal de Santa Maria Bortoli, Marco; Università degli Studi di Padova, Scienze Chimiche Teixeira da Rocha, Joao; Universidade Federal de Santa Maria Orian, Laura; Università degli Studi di Padova, Scienze Chimiche
Key Words:	methylmercury, ligand substitution, reaction mechanism, DFT calculations, activation strain analysis, benchmark, in silico toxicology, Rabenstein's reactions, selenium, selenoproteins

Note: The following files were submitted by the author for peer review, but cannot be converted to PDF. You must view these files (e.g. movies) online.

SupportingInformation2.mp4

FOR TABLE OF CONTENTS USE ONLY

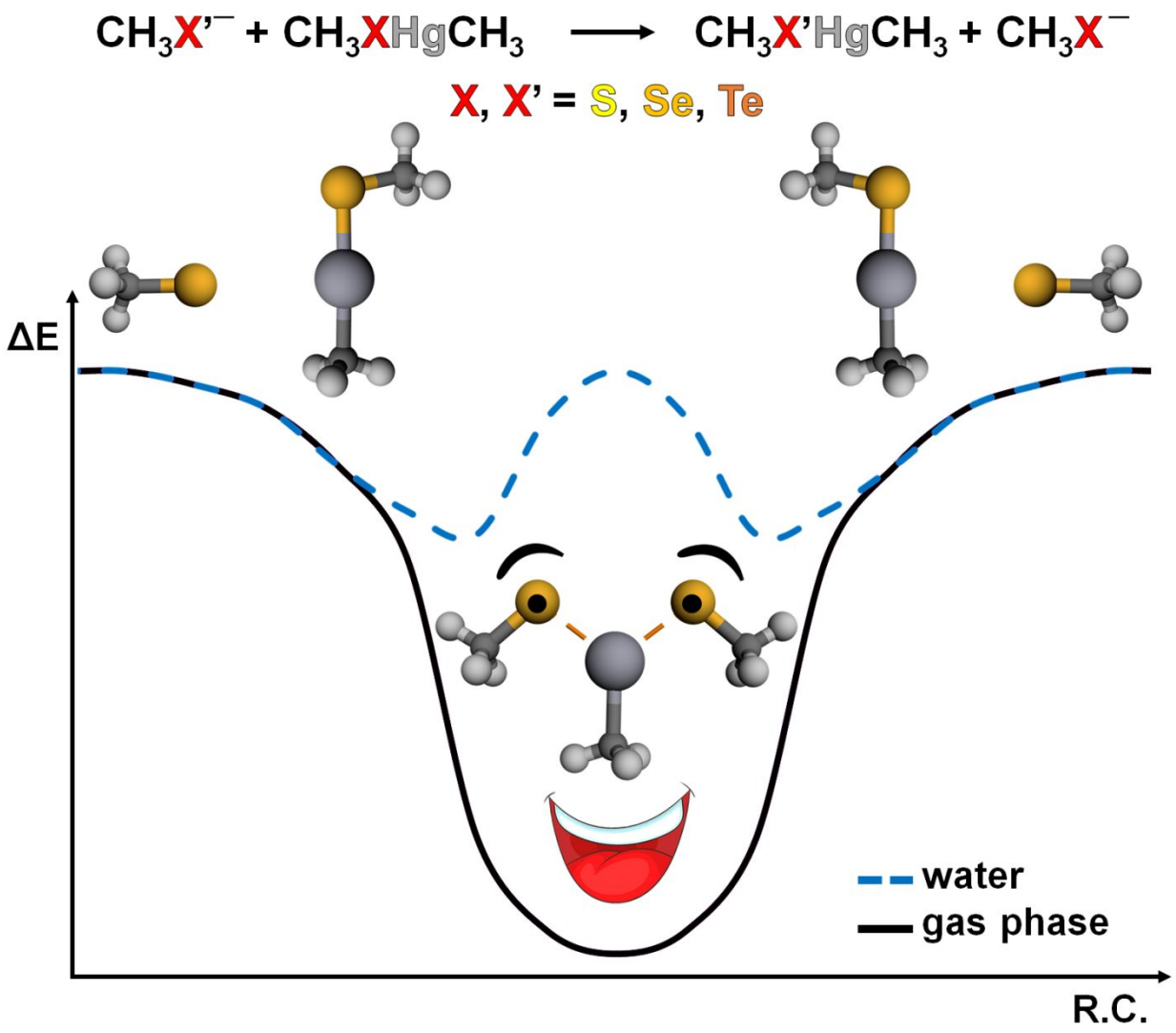

DFT mechanistic investigation on model reactions to understand the chemistry and reactivity of mercury-chalcogen bonds.

♦ SUPPORTING INFORMATION ♦

Chalcogen-mercury bond formation and disruption in model Rabenstein's reactions: a computational analysis

A. Madabeni,[a] M. Dalla Tiezza,[a] O. B. Folorunsho,[b] P. A. Nogara,[a,b] M. Bortoli,[a] J. B. T. Rocha,[b] L. Orian[a*]

[a] Dipartimento di Scienze Chimiche Università degli Studi di Padova Via Marzolo 1 35131 Padova, Italy

[b] Departamento de Bioquímica e Biologia Molecular, Universidade Federal de Santa Maria, Santa Maria RS Brazil

[*] Corresponding author: E-mail: laura.orian@unipd.it

TABLE OF CONTENTS

Table S9. Gibbs free energies relative to free reactants (kcal mol-1) of the stationary points in water 23

Benchmark

Table S1 Cartesian coordinates (Å), energies (E, hartree), and number of imaginary vibrational frequencies (Nimag) of stationary points, computed at the denoted level of level of theory.

ZORA-BLYP/TZ2P-ae

MCYSHG10
E= -3.29982658
Nimag=0

C	-2.641143	3.272876	2.209603
C	-3.118412	1.828284	2.495613
C	-4.444925	1.479651	1.781334
Hg	-5.462259	5.031376	1.450725
N	-3.125989	1.557091	3.929618
O	-5.421173	0.975324	2.295433
O	-4.385278	1.754972	0.428169
S	-3.657908	4.621435	3.004694
H	-3.697230	2.265513	4.398640
H	-3.569024	0.656641	4.117247
H	-5.231783	1.437383	0.047924
C	-7.077259	5.486897	0.119936
H	-6.727317	5.372795	-0.909456
H	-7.903430	4.799421	0.318225
H	-7.394228	6.518269	0.295421
H	-1.649656	3.388776	2.658463
H	-2.557430	3.443356	1.135564
H	-2.371121	1.168006	2.021830

S-
E= -0.84906531
Nimag=0

S	0.000000	0.000000	-0.655629
C	0.000000	0.000000	1.207195
H	-0.512340	0.887399	1.616707
H	-0.512340	-0.887399	1.616707
H	1.024680	0.000000	1.616707

HgS
E= -1.51871409
Nimag=0

C	-0.261190	0.082545	-0.084129
H	-0.472033	-0.933065	-0.430222
H	-1.186661	0.569141	0.234951
H	0.212331	0.659037	-0.883297
Hg	1.081103	-0.022842	1.583964
S	2.592577	-0.062012	3.457411
C	2.792653	-1.879544	3.804529
H	1.842259	-2.343153	4.080643
H	3.235741	-2.404785	2.954711
H	3.477545	-1.942932	4.655568

I2
E= -2.40432468
Nimag=0

C	0.877069	-3.375837	-0.285294
H	1.143938	-4.371213	0.083550
H	-0.211605	-3.285877	-0.363905
H	1.329531	-3.210380	-1.269142
Hg	1.640183	-1.815866	1.131515
S	3.182308	-2.191327	3.204164
C	3.455986	-4.030814	3.156859
H	2.512070	-4.582312	3.244246
H	3.957630	-4.341137	2.232278
H	4.095978	-4.305238	4.005752
S	1.186993	0.750440	1.070504
C	0.078929	0.918883	-0.414454
H	-0.178187	1.979771	-0.532587
H	0.576977	0.580244	-1.330932
H	-0.850700	0.350247	-0.291527

I1
E= -2.40633897
Nimag=0

C	0.902443	-3.399411	-0.128866
H	0.583667	-4.129698	0.622108
H	0.103802	-3.243488	-0.861146
H	1.802262	-3.766247	-0.634454
Hg	1.392068	-1.490000	0.894320
S	3.054465	-1.824770	3.020464
C	3.321498	-3.663902	2.976774
H	2.375237	-4.212122	3.067612
H	3.814051	-3.978675	2.048039
H	3.964935	-3.948696	3.819881
S	0.971731	1.001166	0.830122
C	1.954357	1.642678	2.269186
H	1.600943	1.209659	3.209813
H	3.016684	1.407170	2.154922
H	1.826335	2.732009	2.301781

I3
E= -2.40412782
Nimag=0

C	0.984302	-3.284360	-0.102030
H	0.943043	-4.109469	0.614912
H	0.009428	-3.145407	-0.581037
H	1.742795	-3.492440	-0.864438
Hg	1.564916	-1.439474	0.997503
S	1.541089	1.084912	0.696375
C	1.821330	1.807933	2.384004
H	1.245429	1.268982	3.141896
H	2.880469	1.777484	2.658929
H	1.489495	2.853472	2.359121
S	2.556855	-2.190942	3.412776
C	3.737643	-0.898743	4.037540
H	3.208674	-0.057037	4.500671
H	4.390347	-1.356375	4.792894

H	4.368316	-0.509761	3.229893

ZORA-BLYP/TZ2P

S-
E= -0.85054579
Nimag=0

S	0.000000	0.000000	-0.654925
C	0.000000	0.000000	1.207733
H	-0.512266	0.887270	1.616294
H	-0.512266	-0.887270	1.616294
H	1.024532	0.000000	1.616294

HgS
E= -1.52147387
Nimag=0

C	-0.257627	0.080780	-0.079562
H	-0.470652	-0.935134	-0.423201
H	-1.183116	0.569430	0.235980
H	0.215585	0.653408	-0.881547
Hg	1.081834	-0.021151	1.586638
S	2.589227	-0.060072	3.457376
C	2.790418	-1.877724	3.800998
H	1.840189	-2.342515	4.075058
H	3.233933	-2.400856	2.950307
H	3.474537	-1.943777	4.652083

I2
E= -2.40803797
Nimag=0

C	0.888667	-3.380765	-0.269936
H	1.144392	-4.371579	0.118208
H	-0.198094	-3.288387	-0.367880
H	1.355728	-3.235778	-1.250088
Hg	1.638687	-1.804041	1.129561
S	3.182161	-2.187394	3.197596
C	3.446403	-4.027430	3.140973
H	2.499782	-4.574149	3.226782
H	3.944341	-4.335504	2.213872
H	4.086138	-4.310609	3.986751
S	1.187966	0.752967	1.071446
C	0.077712	0.920134	-0.411453
H	-0.179994	1.980416	-0.530547
H	0.574367	0.580462	-1.327995
H	-0.851155	0.351240	-0.286263

I1
E= -2.41001656
Nimag=0

C	1.017006	-3.337134	-0.212387
H	1.799578	-4.067264	0.015633
H	0.051086	-3.714312	0.140992
H	0.968129	-3.165924	-1.292599
Hg	1.467090	-1.436666	0.837666
S	2.934258	-1.768842	3.097027
C	3.154070	-3.613942	3.110791
H	2.194658	-4.134087	3.223661
H	3.633206	-3.970789	2.190483
H	3.795016	-3.888601	3.958668
S	1.104841	1.057162	0.712192
C	1.979655	1.697829	2.218970
H	1.545916	1.279116	3.131804
H	3.043578	1.444804	2.191695
H	1.867568	2.788977	2.232827

I3
E= -2.40780601
Nimag=0

C	0.980692	-3.283948	-0.100945
H	1.094128	-4.137431	0.573332
H	-0.057816	-3.201572	-0.438123
H	1.638256	-3.405206	-0.968372
Hg	1.566743	-1.443888	0.999390
S	1.475276	1.073619	0.697455
C	1.837298	1.819248	2.358657
H	1.230670	1.352705	3.140431
H	2.893850	1.713014	2.621858
H	1.589159	2.886519	2.305785
S	2.657108	-2.244013	3.344872
C	3.723673	-0.905272	4.067870
H	3.121787	-0.104623	4.513225
H	4.351604	-1.345126	4.853778
H	4.381704	-0.465253	3.309797

ZORA-BLYP-D3(BJ)/TZ2P-ae

S-
E= -0.85418002
Nimag=0

S	0.000000	0.000000	-0.654661
C	0.000000	0.000000	1.207296
H	-0.512359	0.887432	1.616351
H	-0.512359	-0.887432	1.616351
H	1.024719	0.000000	1.616351

HgS
E= -1.53578744
Nimag=0

C	-0.243644	0.067172	-0.070393
H	-0.214431	-0.873263	-0.627057
H	-1.239285	0.224211	0.352203
H	0.021764	0.899108	-0.728308
Hg	1.184365	-0.027399	1.521836
S	2.798042	-0.076813	3.300966
C	2.744298	-1.863374	3.814807
H	1.753056	-2.144587	4.178429
H	3.047013	-2.522933	2.997960
H	3.463148	-1.959732	4.633684

I2
E= -2.43468957
Nimag=0

C	1.034511	-3.522566	-0.044858
H	0.528109	-4.202515	0.648144

H	0.378053	-3.290786	-0.889126
H	1.956943	-3.990600	-0.403855
Hg	1.578419	-1.673848	1.065690
S	3.235535	-2.151646	3.086506
C	3.378306	-3.992976	2.883129
H	2.403810	-4.484416	2.992366
H	3.786643	-4.256596	1.899852
H	4.052836	-4.385837	3.655049
S	1.157688	0.823375	1.082604
C	0.003998	1.009660	-0.363651
H	-0.254646	2.071956	-0.460911
H	0.475691	0.678473	-1.295636
H	-0.918795	0.437906	-0.214275

I1
E= -2.43867874
Nimag=0

C	0.973729	-3.422480	-0.003920
H	0.543682	-4.055899	0.778793
H	0.294704	-3.372987	-0.860600
H	1.938243	-3.837659	-0.313914
Hg	1.325239	-1.419570	0.844457
S	3.032274	-1.726339	2.952602
C	3.225911	-3.569701	2.843976
H	2.263673	-4.081544	2.970445
H	3.646665	-3.871921	1.876796
H	3.904510	-3.910618	3.636851
S	0.941283	1.044098	0.851037
C	1.992975	1.557714	2.289367
H	1.657672	1.067753	3.207606
H	3.039124	1.289278	2.118463
H	1.904792	2.645551	2.398597

I3
E= -2.43706152
Nimag=0

C	0.972836	-3.161623	-0.138858
H	-0.103812	-3.253304	0.039872
H	1.145271	-2.594442	-1.058217
H	1.421238	-4.157562	-0.213493
Hg	1.864312	-2.022622	1.526819
S	2.004918	0.633379	0.898411
C	1.521978	1.438986	2.501583
H	0.554293	1.945112	2.392158
H	1.438410	0.693735	3.299874
H	2.272683	2.182898	2.798972
S	2.829281	-2.025510	3.854319
C	3.970494	-0.560304	3.843695
H	3.716725	0.109692	4.673073
H	5.005177	-0.902936	3.961825
H	3.870327	-0.016727	2.898977

ZORA-BLYP-D3(BJ)/TZ2P

MCYSHG10
E= -3.34216200
Nimag=0

C	-2.507452	3.251383	2.224856
C	-3.179817	1.880428	2.476031
C	-4.467885	1.726262	1.644771
Hg	-5.340810	4.925087	1.517073
N	-3.359569	1.648471	3.902472
O	-5.579860	1.502845	2.078693
O	-4.216372	1.852636	0.294107
S	-3.406673	4.711773	2.943575
H	-3.838926	2.457857	4.306729
H	-3.962950	0.840656	4.059103
H	-5.071778	1.702075	-0.160772
C	-7.071241	5.166590	0.284848
H	-6.757325	5.223142	-0.760613
H	-7.726510	4.306208	0.441201
H	-7.583454	6.088419	0.571970
H	-1.543395	3.250872	2.742085
H	-2.334858	3.400220	1.158346
H	-2.486691	1.123143	2.074506

S-
E= -0.85566128
Nimag=0

S	0.000000	0.000000	-0.653965
C	0.000000	0.000000	1.207837
H	-0.512285	0.887304	1.615939
H	-0.512285	-0.887304	1.615939
H	1.024571	0.000000	1.615939

HgS
E= -1.53855950
Nimag=0

C	-0.240118	0.065390	-0.066071
H	-0.210897	-0.875054	-0.622557
H	-1.236510	0.221923	0.354685
H	0.023281	0.896293	-0.725933
Hg	1.185914	-0.025927	1.523621
S	2.796238	-0.074979	3.299669
C	2.741886	-1.861616	3.811703
H	1.750441	-2.142900	4.174244
H	3.044116	-2.520318	2.994198
H	3.459977	-1.960421	4.630570

I2
E= -2.43845801
Nimag=0

C	1.030738	-3.494849	-0.090513
H	1.169690	-4.377113	0.541295
H	-0.012078	-3.424976	-0.415637
H	1.683089	-3.564509	-0.967570
Hg	1.592509	-1.689610	1.077444
S	3.195071	-2.154210	3.129124
C	3.336805	-3.997850	2.953418
H	2.357454	-4.484077	3.039090
H	3.774502	-4.275256	1.987127
H	3.984654	-4.383131	3.751013
S	1.175623	0.809785	1.081589

C	0.050663	0.988264	-0.387488
H	-0.213427	2.048173	-0.492509
H	0.542836	0.658358	-1.309104
H	-0.871027	0.410584	-0.256250

I1
E= -2.44239912
Nimag=0

C	0.976417	-3.420143	-0.000955
H	0.549197	-4.055371	0.781648
H	0.295893	-3.373566	-0.856431
H	1.940262	-3.835035	-0.312949
Hg	1.325719	-1.419800	0.845379
S	3.031324	-1.724011	2.950939
C	3.225626	-3.566826	2.842579
H	2.263791	-4.078757	2.969703
H	3.645421	-3.868843	1.875196
H	3.904724	-3.907793	3.634536
S	0.940099	1.038281	0.850773
C	1.990793	1.554401	2.288314
H	1.656365	1.064328	3.206581
H	3.037033	1.286997	2.117588
H	1.901814	2.641814	2.397655

I3
E= -2.44068611
Nimag=0

C	0.992300	-3.218843	-0.075346
H	0.659135	-3.916844	0.697736
H	0.178340	-3.008090	-0.776410
H	1.841258	-3.648248	-0.617802
Hg	1.651628	-1.373666	0.929252
S	2.234048	1.065370	0.773939
C	1.876742	1.700456	2.481913
H	1.614701	0.867976	3.142048
H	2.762898	2.209001	2.877641
H	1.043241	2.410882	2.439591
S	2.104170	-1.866802	3.577710
C	3.643193	-0.879316	3.904999
H	3.499645	-0.219986	4.770743
H	4.484195	-1.551980	4.115084
H	3.898638	-0.261137	3.037911

ZORA-B3LYP/TZ2P-ae
MCYSHG10
E= -4.01341766
Nimag=0

C	-2.653130	3.291265	2.233790
C	-3.122842	1.848667	2.473788
C	-4.430186	1.520159	1.744747
Hg	-5.466446	4.988134	1.486084
N	-3.148273	1.539833	3.886257
O	-5.385141	0.973340	2.227066
O	-4.383738	1.869873	0.429471
S	-3.688025	4.595319	3.030295
H	-3.706884	2.234525	4.372597
H	-3.588881	0.642268	4.047485
H	-5.210170	1.559051	0.027162
C	-7.061660	5.420132	0.162328
H	-6.700966	5.366010	-0.862536
H	-7.859527	4.696535	0.312984
H	-7.431307	6.422529	0.366789
H	-1.675154	3.399053	2.699538
H	-2.547944	3.485012	1.171344
H	-2.375289	1.206362	1.989793

S-
E= -1.02151583
Nimag=0

S	0.000000	0.000000	-0.638348
C	0.000000	0.000000	1.204775
H	-0.509246	0.882040	1.611754
H	-0.509246	-0.882040	1.611754
H	1.018492	0.000000	1.611754

HgS
E= -1.81249790
Nimag=0

C	-0.242082	0.073422	-0.059520
H	-0.474427	-0.935494	-0.394212
H	-1.157519	0.578430	0.241027
H	0.234659	0.624980	-0.866957
Hg	1.078911	-0.028470	1.594613
S	2.564698	-0.068675	3.452500
C	2.780918	-1.866328	3.784396
H	1.840124	-2.341664	4.050736
H	3.230514	-2.379775	2.938103
H	3.458531	-1.934036	4.633444

I2
E= -2.87217572
Nimag=0

C	0.856034	-3.425990	-0.325030
H	1.040998	-4.423670	0.071049
H	-0.214227	-3.284508	-0.473819
H	1.366093	-3.316698	-1.282341
Hg	1.617723	-1.897087	1.078897
S	3.143360	-2.296712	3.105774
C	3.399098	-4.117866	3.043154
H	2.456480	-4.660093	3.127836
H	3.891392	-4.423884	2.119197
H	4.035961	-4.407195	3.881597
S	1.161292	0.626629	1.014916
C	0.061390	0.786201	-0.451707
H	-0.205401	1.838261	-0.571289
H	0.556740	0.453541	-1.364700
H	-0.858271	0.212681	-0.329561

I1

E= -2.87465547
Nimag=0

C	0.909301	-3.386825	-0.075348
H	0.533287	-4.083343	0.673661
H	0.161902	-3.252734	-0.856153
H	1.820793	-3.794878	-0.512085
Hg	1.378553	-1.481226	0.896082
S	3.047698	-1.824636	2.966740
C	3.286899	-3.647364	2.920312
H	2.343874	-4.180599	3.053267
H	3.729982	-3.971248	1.976919
H	3.959274	-3.940498	3.729424
S	0.976337	0.971080	0.855027
C	1.978709	1.591961	2.263001
H	1.651766	1.149067	3.201770
H	3.033356	1.362121	2.124198
H	1.851454	2.674587	2.313877

I3
E= -2.87221555
Nimag=0

C	1.124840	-3.276648	0.065204
H	0.429501	-3.823435	0.700660
H	0.694361	-3.140685	-0.926156
H	2.052639	-3.842728	-0.014012
Hg	1.562349	-1.360673	1.020788
S	1.814694	1.092423	0.677001
C	1.837985	1.824567	2.363157
H	1.623208	1.061416	3.110269
H	2.815349	2.263254	2.568404
H	1.082769	2.609373	2.422863
S	1.982989	-1.727701	3.687974
C	3.676831	-1.055846	3.933150
H	3.882695	-0.980845	5.003124
H	4.431264	-1.707548	3.487979
H	3.783594	-0.063078	3.494165

ZORA-B3LYP-D3(BJ)/TZ2P-ae

MCYSHG10
E= -4.04879219
Nimag=0

C	-2.517965	3.246103	2.216131
C	-3.189384	1.886470	2.463097
C	-4.466395	1.739819	1.636207
Hg	-5.331455	4.909926	1.524431
N	-3.373745	1.652654	3.875334
O	-5.565116	1.506607	2.066517
O	-4.225459	1.887908	0.306826
S	-3.408444	4.694778	2.919761
H	-3.837149	2.456219	4.288292
H	-3.969974	0.849982	4.033217
H	-5.066253	1.738352	-0.153112
C	-7.052278	5.151412	0.319250
H	-6.753986	5.243392	-0.722659
H	-7.693122	4.282426	0.448934
H	-7.583081	6.049193	0.627667
H	-1.560115	3.240688	2.732571
H	-2.338259	3.390370	1.155781
H	-2.503385	1.131768	2.060740

S-
E= -1.02567850
Nimag=0

S	0.000000	0.000000	-0.637670
C	0.000000	0.000000	1.204864
H	-0.509261	0.882066	1.611498
H	-0.509261	-0.882066	1.611498
H	1.018522	0.000000	1.611498

HgS
E= -1.82676266
Nimag=0

C	-0.237553	0.052650	-0.030215
H	-0.449958	-0.958968	-0.369584
H	-1.162279	0.538303	0.273287
H	0.228526	0.617312	-0.834663
Hg	1.084667	-0.031955	1.621278
S	2.570688	-0.070062	3.474167
C	2.752598	-1.873011	3.791907
H	1.801885	-2.330533	4.053449
H	3.190115	-2.386668	2.939665
H	3.428979	-1.963221	4.639483

I2
E= -2.89783042
Nimag=0

C	0.729354	-3.147922	-0.422372
H	0.943797	-4.211729	-0.333268
H	-0.346405	-2.984666	-0.363127
H	1.090673	-2.780697	-1.382617
Hg	1.701458	-1.998982	1.178284
S	3.182411	-2.312032	3.166593
C	3.459455	-4.130166	3.146048
H	2.522939	-4.677712	3.251301
H	3.946689	-4.449144	2.224720
H	4.106798	-4.388699	3.986153
S	1.186944	0.563171	1.021163
C	0.115518	0.541487	-0.472679
H	-0.202612	1.560956	-0.699642
H	0.647272	0.147912	-1.340169
H	-0.775631	-0.068165	-0.316416

I1
E= -2.90199251
Nimag=0

C	0.978757	-3.400369	0.015405
H	0.545303	-4.035232	0.787671
H	0.306704	-3.354838	-0.840012
H	1.934489	-3.823742	-0.292125
Hg	1.334055	-1.424726	0.859343

S	3.019714	-1.735895	2.931513
C	3.223887	-3.559138	2.832764
H	2.270504	-4.075352	2.957387
H	3.647284	-3.862540	1.873775
H	3.898204	-3.893094	3.623943
S	0.952064	1.007571	0.862209
C	1.988069	1.537409	2.280730
H	1.658887	1.058950	3.200513
H	3.031407	1.276921	2.116761
H	1.895149	2.619752	2.380678

I3
E= -2.89992562
Nimag=0

C	0.989618	-3.198750	-0.058884
H	0.477365	-3.824639	0.670048
H	0.322407	-2.969434	-0.888663
H	1.864013	-3.730299	-0.433801
Hg	1.653221	-1.385713	0.951766
S	2.197286	1.035401	0.792100
C	1.868021	1.671740	2.484386
H	1.612687	0.851054	3.152135
H	2.754650	2.177510	2.867033
H	1.041187	2.381758	2.451876
S	2.165348	-1.889609	3.543922
C	3.651687	-0.861552	3.882029
H	3.474598	-0.195843	4.729227
H	4.503561	-1.501297	4.119508
H	3.908483	-0.251553	3.016327

ZORA-M06-2X/TZ2P-ae
MCYSHG10
E= -4.97706242
Nimag=0

C	-2.509846	3.239559	2.213420
C	-3.197869	1.887478	2.444510
C	-4.494609	1.810635	1.648013
Hg	-5.311207	4.874511	1.528654
N	-3.364564	1.629869	3.852113
O	-5.587739	1.607417	2.097163
O	-4.286509	2.012775	0.326766
S	-3.396099	4.676898	2.916167
H	-3.825810	2.425970	4.281622
H	-3.962230	0.826574	4.000828
H	-5.138837	1.906123	-0.119866
C	-7.010870	5.082347	0.331139
H	-6.721119	5.289703	-0.695722
H	-7.587260	4.161193	0.370338
H	-7.622479	5.900962	0.701610
H	-1.556760	3.214371	2.737580
H	-2.318866	3.386529	1.154762
H	-2.542891	1.125152	2.009886

S-
E= -1.25027436
Nimag=0

S	0.000000	0.000000	-0.627989
C	0.000000	0.000000	1.202524
H	-0.508237	0.880293	1.609051
H	-0.508237	-0.880293	1.609051
H	1.016475	0.000000	1.609051

HgS
E= -2.20095445
Nimag=0

C	-0.238885	0.004602	-0.019355
H	-0.464089	-1.000504	-0.367496
H	-1.166802	0.509029	0.237835
H	0.259960	0.553295	-0.814225
Hg	1.003761	-0.093102	1.659803
S	2.407066	-0.152997	3.552893
C	2.564525	-1.948269	3.859174
H	1.603240	-2.404045	4.079141
H	3.032827	-2.458865	3.022410
H	3.205059	-2.053879	4.731419

I2
E= -3.49599358
Nimag=0

C	1.112650	-3.521188	0.019379
H	0.845242	-4.269294	0.764412
H	0.299533	-3.417467	-0.696247
H	2.005499	-3.861067	-0.504496
Hg	1.554506	-1.659276	1.028377
S	3.212626	-2.149861	3.030175
C	3.283129	-3.966601	2.839689
H	2.337973	-4.435358	3.117512
H	3.510595	-4.255052	1.812698
H	4.063034	-4.371166	3.486127
S	1.148255	0.785077	1.071226
C	0.031701	1.001959	-0.359611
H	-0.225920	2.058405	-0.438874
H	0.508075	0.696322	-1.289995
H	-0.889799	0.434153	-0.239345

I1
E= -3.50109611
Nimag=0

C	1.037167	-3.379904	0.018967
H	0.815657	-4.058577	0.841452
H	0.230281	-3.420517	-0.709948
H	1.960663	-3.708526	-0.456903
Hg	1.317414	-1.402894	0.806864
S	2.994661	-1.699600	2.923054
C	3.148618	-3.518699	2.842478
H	2.222681	-4.011365	3.143857
H	3.393079	-3.857391	1.834616
H	3.941119	-3.853254	3.513236
S	0.969980	1.015375	0.850892
C	2.005999	1.481911	2.278056
H	1.668090	0.981953	3.183001

H	3.044747	1.205965	2.110416
H	1.934320	2.561200	2.410518

I3
E= -3.49927889
Nimag=0

C	1.047275	-3.240530	-0.027617
H	0.656239	-3.919871	0.727366
H	0.294122	-3.076857	-0.795933
H	1.924362	-3.697107	-0.483918
Hg	1.624756	-1.410621	0.940048
S	1.932533	1.040654	0.863132
C	1.704263	1.571786	2.596136
H	0.843345	2.235902	2.660339
H	1.544823	0.711125	3.243969
H	2.589102	2.107193	2.938395
S	2.450448	-1.952495	3.456363
C	3.759834	-0.710072	3.743004
H	3.508392	-0.068591	4.589349
H	4.705351	-1.207445	3.961168
H	3.899286	-0.074295	2.867207

ZORA-OLYP/TZ2P-ae

MCYSHG10

E= -3.34688446
Nimag=0

C	-2.705007	3.279390	2.193117
C	-3.131104	1.827572	2.503589
C	-4.435880	1.415568	1.793180
Hg	-5.472500	5.083070	1.443433
N	-3.116253	1.576415	3.930338
O	-5.435932	0.994907	2.329042
O	-4.326043	1.524639	0.432694
S	-3.706553	4.612453	2.972124
H	-3.729159	2.248605	4.387653
H	-3.511261	0.660518	4.124072
H	-5.166948	1.190582	0.075130
C	-7.049495	5.585513	0.130224
H	-6.790814	5.261478	-0.880897
H	-7.964506	5.084808	0.454888
H	-7.197064	6.668009	0.139871
H	-1.707128	3.417061	2.619052
H	-2.632429	3.429761	1.116117
H	-2.357486	1.197719	2.035353

S-
E= -0.85887720
Nimag=0

S	0.000000	0.000000	1.096988
C	0.000000	0.000000	2.929374
H	-0.510643	-0.884460	3.348164
H	1.021287	0.000000	3.348164
H	-0.510643	0.884460	3.348164

HgS
E= -1.53532891
Nimag=0

C	-0.238935	0.073335	-0.055327
H	-0.487865	-0.940624	-0.378606
H	-1.152184	0.598050	0.235521
H	0.248299	0.607983	-0.874293
Hg	1.073635	-0.026495	1.599841
S	2.550201	-0.070476	3.460603
C	2.779961	-1.862257	3.778928
H	1.841325	-2.354865	4.043474
H	3.241150	-2.373123	2.930394
H	3.458739	-1.929139	4.633593

I1
E= -2.42683730
Nimag=0

C	-0.175734	-0.909489	0.260107
H	0.405826	-1.806865	0.025350
H	-0.846612	-1.131785	1.096190
H	-0.769229	-0.624460	-0.614035
Hg	1.188726	0.713777	0.832954
S	2.706697	0.223256	2.976201
C	2.201755	-1.474794	3.439493
H	1.135105	-1.535547	3.688300
H	2.404226	-2.198508	2.640354
H	2.770591	-1.785953	4.325038
C	3.075864	3.612265	1.204781
H	3.371255	4.620325	0.890224
H	2.700451	3.660690	2.230897
H	3.959076	2.967427	1.192263
S	1.790948	3.015660	0.045800

I2
E= -2.42527347
Nimag=0

C	-0.156329	-0.841701	0.048634
H	0.419164	-1.720099	-0.262165
H	-0.896214	-1.150429	0.794635
H	-0.672837	-0.422800	-0.820481
Hg	1.206556	0.652846	0.937159
S	2.668232	0.277859	3.037337
C	2.263223	-1.445709	3.510070
H	1.199593	-1.570051	3.746127
H	2.523979	-2.162179	2.721928
H	2.839910	-1.706387	4.406507
C	0.650204	3.268358	-1.274057
H	0.897727	2.555704	-2.069617
H	-0.413457	3.156911	-1.032599
H	0.802230	4.280828	-1.668674
S	1.718165	3.055327	0.200044

I3
E= -2.42442215
Nimag=0

C	-0.120680	0.525632	-0.350870
H	-0.149494	-0.144226	-1.216566
H	-1.133687	0.873280	-0.130289

H	0.524459	1.379768	-0.579812
Hg	0.647532	-0.579972	1.390490
S	2.928158	-1.229594	2.228951
C	2.775011	-1.817088	3.955445
H	2.230116	-1.102583	4.579280
H	2.270960	-2.785976	4.014214
H	3.787630	-1.927841	4.361588
C	-1.083158	-2.657773	4.015035
H	-2.023803	-3.058942	4.413986
H	-0.548783	-3.481019	3.527532
H	-0.478811	-2.310589	4.860777
S	-1.473214	-1.306646	2.843077

ZORA-OLYP/TZ2P

I1

E=-2.43041444

C	-0.170449	-0.905384	0.263681
H	0.408277	-1.803380	0.025184
H	-0.841000	-1.131481	1.098754
H	-0.765870	-0.619382	-0.608563
Hg	1.193358	0.711614	0.838941
S	2.705432	0.218342	2.977109
C	2.198580	-1.478385	3.438172
H	1.132015	-1.538188	3.686182
H	2.400448	-2.201403	2.638685
H	2.765952	-1.791698	4.323406
C	3.074414	3.614737	1.201795
H	3.366652	4.621515	0.881521
H	2.700480	3.668543	2.227903
H	3.959722	2.973192	1.192333
S	1.790931	3.007357	0.048816

I2

E -2.42894374 Hartree

Nimag=

0C	-0.149932	-0.830770	0.047694
H	0.419762	-1.714971	-0.256530
H	-0.898367	-1.133509	0.787314
H	-0.657646	-0.412580	-0.826622
Hg	1.213593	0.653491	0.940687
S	2.672173	0.274361	3.032959
C	2.261590	-1.445748	3.508703
H	1.198137	-1.565768	3.746311
H	2.518267	-2.164372	2.721628
H	2.837961	-1.707840	4.404467
C	0.646236	3.259952	-1.270876
H	0.893971	2.547786	-2.066410
H	-0.416231	3.144947	-1.027191
H	0.793099	4.272121	-1.667180
S	1.717534	3.051378	0.199894

I3

E=-2.42803077

Nimag=0

C	-0.115870	0.528100	-0.353575
H	-0.086846	-0.123810	-1.232670
H	-1.148825	0.834590	-0.168360
H	0.502985	1.410304	-0.544647
Hg	0.631496	-0.576623	1.392955
S	2.916157	-1.177852	2.242695
C	2.768442	-1.830357	3.944791
H	2.231514	-1.137717	4.599208
H	2.259258	-2.797564	3.969178
H	3.781803	-1.962959	4.341480
C	-1.077765	-2.648316	4.031210
H	-2.012843	-3.042708	4.448475
H	-0.533770	-3.485743	3.580492
H	-0.477992	-2.256534	4.859846
S	-1.485507	-1.356378	2.801761

Gas Phase

Table S2 Cartesian coordinates (Å), energies (E, Hartree), and number of imaginary vibrational frequencies (Nimag) of stationary points, computed at ZORA-OLYP/TZ2P.

Reactants/products

HgSe
E=-1.51264442
Nimag=0

C	-0.002994	0.042475	0.192792
H	-0.264310	-0.984929	-0.070489
H	-0.881840	0.554719	0.591463
H	0.353646	0.569608	-0.695367
Hg	1.528424	0.032644	1.657235
Se	3.367647	0.027428	3.336050
C	2.316988	-0.149275	5.009859
H	1.651376	0.703267	5.145135
H	1.754870	-1.083101	5.021572
H	3.055273	-0.162155	5.813870

HgS
E=-1.53858225
Nimag=0

C	-0.237219	0.073743	-0.053178
H	-0.487283	-0.938491	-0.380345
H	-1.151057	0.597354	0.237174
H	0.248221	0.610040	-0.871908
Hg	1.072970	-0.030032	1.598205
S	2.546581	-0.072914	3.454079
C	2.779726	-1.861780	3.778929
H	1.842432	-2.355279	4.045359
H	3.241353	-2.375056	2.932466
H	3.458603	-1.925195	4.633348

HgTe
E=-1.48560058
Nimag=0

C	-0.048407	0.040636	0.121423
H	-0.150315	-0.923673	-0.381388
H	-0.978330	0.285058	0.640389
H	0.177526	0.818640	-0.611419
Hg	1.535635	-0.066603	1.542690
Te	3.544715	-0.202001	3.305484
C	2.329279	-0.110240	5.118793
H	1.780582	0.829621	5.156452
H	1.652383	-0.962188	5.161275
H	3.036012	-0.158567	5.948422

S-
E=-0.86002017
Nimag=0

S	0.000000	0.000000	1.098218
C	0.000000	0.000000	2.929496
H	-0.510471	-0.884161	3.347714
H	1.020941	0.000000	3.347714
H	-0.510471	0.884161	3.347714

Te-
E=-0.82088156
Nimag=0

Te	3.772403	3.002533	0.000000
C	2.711408	4.942509	0.000000
H	2.082440	5.020151	-0.891066
H	2.082440	5.020151	0.891066
H	3.436266	5.761208	0.000000

Se-
E=-0.83839606
Nimag=0

Se	0.000000	0.000000	0.983406
C	0.000000	0.000000	2.978921
H	-0.512748	-0.888106	3.369510
H	1.025496	0.000000	3.369510
H	-0.512748	0.888106	3.369510

TCIs

SHgS-
E=-2.42894374
Nimag=0

C	-0.149932	-0.830770	0.047694
H	0.419762	-1.714971	-0.256530
H	-0.898367	-1.133509	0.787314
H	-0.657646	-0.412580	-0.826622
Hg	1.213593	0.653491	0.940687
S	2.672173	0.274361	3.032959
C	2.261590	-1.445748	3.508703
H	1.198137	-1.565768	3.746311
H	2.518267	-2.164372	2.721628
H	2.837961	-1.707840	4.404467
C	0.646236	3.259952	-1.270876
H	0.893971	2.547786	-2.066410
H	-0.416231	3.144947	-1.027191
H	0.793099	4.272121	-1.667180
S	1.717534	3.051378	0.199894

SHgSe-
E=-2.40538742
Nimag=0

C	0.695284	0.050133	0.250519
H	0.240139	-0.923785	0.454585
H	-0.075160	0.825962	0.305612
H	1.118635	0.045870	-0.758965

Hg	2.285659	0.490606	1.714113
S	3.110674	-0.834923	3.734221
C	2.053677	-2.330610	3.707968
H	0.990299	-2.086258	3.811439
H	2.184236	-2.911854	2.788007
H	2.336580	-2.969589	4.553352
C	3.041036	3.623409	0.052183
H	1.979606	3.838920	0.198170
H	3.577585	4.565884	-0.093236
H	3.162402	3.005188	-0.840837
Se	3.807972	2.722023	1.648759

SHgTe-
E=-2.38262223
Nimag=0

C	-0.123373	-0.770789	0.057748
H	0.409382	-1.662798	-0.287813
H	-0.913841	-1.078321	0.750212
H	-0.571645	-0.262324	-0.800024
Hg	1.285571	0.575172	1.096533
S	2.710338	0.143238	3.170375
C	2.287346	-1.583520	3.611677
H	1.222701	-1.700595	3.843716
H	2.544291	-2.287933	2.812436
H	2.860004	-1.862521	4.504448
C	0.532218	3.345258	-1.474035
H	0.831607	2.584075	-2.195983
H	-0.502684	3.181475	-1.170058
H	0.628706	4.335455	-1.925302
Te	1.849525	3.272607	0.280920

SeHgSe-
E=-2.38173093
Nimag=0

C	0.716343	0.030730	0.281043
H	0.291503	-0.945353	0.532832
H	-0.071284	0.789819	0.325941
H	1.117615	-0.001203	-0.736995
Hg	2.330142	0.560554	1.693022
Se	3.205069	-0.835182	3.806086
C	1.998485	-2.412124	3.717215
H	0.953197	-2.108993	3.815062
H	2.131089	-2.952025	2.776464
H	2.254541	-3.077103	4.547558
C	3.041940	3.683614	0.012493
H	1.979172	3.888185	0.163569
H	3.568344	4.631220	-0.136481
H	3.166250	3.064651	-0.879483
Se	3.826219	2.794187	1.607566

SeHgTe-
E= -2.35894248
Nimag=0

C	0.741762	0.032646	0.313439
H	0.259053	-0.917501	0.560476
H	-0.004045	0.833482	0.328825
H	1.173441	-0.030194	-0.690378
Hg	2.340667	0.492029	1.768968
Se	3.182850	-0.931510	3.861129
C	1.968796	-2.500947	3.744311
H	0.924720	-2.193538	3.840450
H	2.104910	-3.029092	2.797557
H	2.217622	-3.177058	4.567737
C	3.023135	3.794518	-0.094398
H	1.960529	3.968226	0.081122
H	3.524903	4.747659	-0.276701
H	3.154313	3.140996	-0.958011
Te	3.935967	2.881260	1.681367

TeHgTe-
E= -2.33593302
Nimag=0

C	0.781370	0.052526	0.338021
H	0.296089	-0.877413	0.647169
H	0.041861	0.858786	0.310779
H	1.206234	-0.074326	-0.662734
Hg	2.398871	0.585709	1.752065
Te	3.299027	-0.952199	3.976026
C	1.905539	-2.637193	3.780542
H	0.877924	-2.281495	3.866743
H	2.049705	-3.129529	2.817870
H	2.118428	-3.341391	4.588149
C	3.007072	3.866072	-0.159167
H	1.943290	4.024663	0.022954
H	3.492704	4.825204	-0.353324
H	3.142937	3.206568	-1.017393
Te	3.947572	2.984996	1.618192

Table S3 Cartesian coordinates (Å), energies (E, Hartree), and number of imaginary vibrational frequencies (Nimag) of stationary points, computed at ZORA-BLYP-D3(BJ)/TZ2P.

Reactants/products

HgSe
E= -1.51448790
Nimag=0

C	-0.254675	-0.035148	-0.156681
H	-0.144923	-0.925393	-0.781155
H	-1.250658	-0.008112	0.292061
H	-0.086070	0.864603	-0.754169
Hg	1.214521	-0.100508	1.407058
Se	2.944645	-0.148012	3.235550
C	2.742469	-2.078716	3.774820
H	1.731082	-2.266567	4.135908
H	2.987029	-2.732787	2.937571
H	3.459534	-2.228256	4.584575

HgTe
E= -1.49061818
Nimag=0

C	-0.312942	0.086212	-0.152488
H	-0.266555	-0.890608	-0.640604
H	-1.306739	0.252897	0.269968
H	-0.066545	0.875944	-0.866864
Hg	1.140406	0.128657	1.443504
Te	2.958535	0.179077	3.438665
C	2.799740	-1.980156	3.905426
H	1.781724	-2.210772	4.216887
H	3.090675	-2.563190	3.032504
H	3.496028	-2.155671	4.727132

Se-
E= -0.83580489
Nimag=0

Se	0.000000	0.000000	-0.771347
C	0.000000	0.000000	1.258003
H	-0.514639	0.891381	1.638344
H	-0.514639	-0.891381	1.638344
H	1.029278	0.000000	1.638344

Te-
E= -0.82064671
Nimag=0

Te	0.000000	0.000000	-0.931235
C	0.000000	0.000000	1.312179
H	-0.516214	0.894109	1.673582
H	-0.516214	-0.894109	1.673582
H	1.032429	0.000000	1.673582

TCIs

SHgSe-
E= -2.41691814
Nimag=0

C	1.035003	-3.477491	-0.030816
H	0.527052	-4.155622	0.662378
H	0.379692	-3.247965	-0.876531
H	1.956445	-3.948184	-0.387944
Hg	1.579087	-1.627733	1.074123
S	1.129523	0.863239	1.052413
C	-0.022122	1.010695	-0.399539
H	-0.296219	2.066866	-0.515375
H	0.457238	0.671223	-1.324357
H	-0.936666	0.427953	-0.243547
Se	3.305525	-2.089728	3.177792
C	3.404109	-4.085157	2.897132
H	2.409308	-4.527080	2.996912
H	3.799179	-4.304530	1.901795
H	4.069949	-4.506903	3.656595

SHgTe-
E= -2.39722869
Nimag=0

C	1.032139	-3.436354	-0.004880
H	0.538745	-4.110362	0.702251
H	0.369492	-3.229894	-0.850863
H	1.960044	-3.896493	-0.358213
Hg	1.550727	-1.561398	1.069977
S	1.083459	0.922659	0.998474
C	-0.061864	1.042656	-0.461051
H	-0.336941	2.096198	-0.595926
H	0.422674	0.688416	-1.377514
H	-0.976060	0.461261	-0.298634
Te	3.365935	-2.024818	3.325351
C	3.450923	-4.210691	2.919834
H	2.443776	-4.625363	2.988019
H	3.853033	-4.371979	1.918172
H	4.101020	-4.674254	3.666032

SeHgSe-
E= -2.39517182
Nimag=0

C	0.982964	-3.352457	-0.123230
H	1.213888	-4.304943	0.362842
H	-0.095535	-3.265719	-0.288946
H	1.507375	-3.287724	-1.082355
Hg	1.670863	-1.680379	1.186013
Se	1.189998	0.949175	1.114648
C	-0.013138	0.959542	-0.505859
H	-0.330553	1.992014	-0.683223
H	0.530814	0.587641	-1.377466
H	-0.889184	0.332291	-0.324300
Se	3.305770	-2.158078	3.308674
C	3.413085	-4.155593	3.044334
H	2.414246	-4.594856	3.106781
H	3.850324	-4.380584	2.068338

H	4.046185	-4.570748	3.834780

SeHgTe-
E= -2.37544474
Nimag=0

C	0.995903	-3.320021	-0.089952
H	1.089902	-4.240955	0.492465
H	-0.041994	-3.175345	-0.405572
H	1.645539	-3.370121	-0.970023
Hg	1.646121	-1.597880	1.174070
Se	1.135329	1.017180	1.063170
C	-0.072211	1.000185	-0.553994
H	-0.397641	2.028323	-0.741322
H	0.472544	0.623137	-1.422788
H	-0.942952	0.368612	-0.362545
Te	3.394880	-2.091553	3.426374
C	3.459081	-4.283119	3.050296
H	2.445051	-4.682865	3.104366
H	3.880297	-4.462036	2.059723
H	4.087253	-4.743960	3.816763

TeHgTe-
E= -2.35556536
Nimag=0

C	0.938543	-3.187133	-0.124000
H	0.987650	-4.173583	0.346146
H	-0.095887	-2.939322	-0.380263
H	1.556562	-3.173706	-1.027649
Hg	1.729638	-1.648382	1.295749
Te	1.155501	1.147522	1.158244
C	-0.127900	0.972611	-0.650023
H	-0.498327	1.969456	-0.902438
H	0.468295	0.572487	-1.471578
H	-0.962247	0.304792	-0.429924
Te	3.459663	-2.195580	3.503508
C	3.535765	-4.385787	3.123291
H	2.524221	-4.791137	3.179227
H	3.957266	-4.560068	2.132100
H	4.168359	-4.842587	3.888638

Solvent Calculations

Table S4 Cartesian coordinates (Å), energies (E, Hartree), and number of imaginary vibrational frequencies (Nimag) of stationary points, computed at COSMO(water)-ZORA-OLYP/TZ2P.

Reactants/Products

HgS
E=-1.54503284
Nimag=0

C	-0.240623	0.072338	-0.056986
H	-0.507411	-0.945687	-0.350299
H	-1.139027	0.626337	0.224380
H	0.267871	0.576626	-0.881786
Hg	1.055813	-0.017709	1.596863
S	2.530952	-0.070917	3.479463
C	2.786648	-1.863821	3.780577
H	1.847812	-2.364180	4.025022
H	3.250743	-2.349671	2.920305
H	3.461550	-1.940926	4.636590

HgSe
E=-1.51780393
Nimag=0

C	-0.007212	0.043222	0.188476
H	-0.258108	-0.986812	-0.074431
H	-0.882734	0.548792	0.602281
H	0.351228	0.578975	-0.693563
Hg	1.523695	0.029753	1.643704
Se	3.372043	0.019378	3.339986
C	2.320169	-0.148512	5.015963
H	1.654090	0.705610	5.135459
H	1.753527	-1.079307	5.019047
H	3.052383	-0.160419	5.825199

HgTe
E=-1.48945388
Nimag=0

C	-0.053035	0.041939	0.115119
H	-0.159783	-0.931818	-0.368382
H	-0.976159	0.304714	0.637210
H	0.187654	0.806602	-0.627153
Hg	1.527370	-0.060287	1.533481
Te	3.543645	-0.189367	3.309065
C	2.333120	-0.113514	5.126470
H	1.773160	0.819959	5.159595
H	1.662777	-0.971121	5.160804
H	3.040329	-0.156422	5.955913

S-
E=-0.97168186
Nimag=0

S	0.000000	0.000000	1.102676
C	0.000000	0.000000	2.946220
H	-0.511103	-0.885257	3.340654
H	1.022207	0.000000	3.340654
H	-0.511103	0.885257	3.340654

Se-
E=-0.94357865
Nimag=0

Se	0.000000	0.000000	0.990247
C	0.000000	0.000000	2.988347
H	-0.513131	-0.888769	3.364088
H	1.026262	0.000000	3.364088
H	-0.513131	0.888769	3.364088

Te-
E=-0.91377017
Nimag=0

Te	0.000000	0.000000	0.830994
C	0.000000	0.000000	3.037361
H	-0.514549	-0.891225	3.400842
H	1.029098	0.000000	3.400842
H	-0.514549	0.891225	3.400842

Transition States

SHgS-
E= -2.50990543
Nimag=-59.12

C	-0.206585	-1.036681	-0.113725
H	0.107097	-1.143421	-1.155307
H	-0.104517	-1.993909	0.402785
H	-1.248799	-0.708691	-0.079964
Hg	1.028596	0.453220	0.846041
S	2.544926	0.427057	2.969454
C	2.374769	-1.276666	3.634206
H	1.337048	-1.496905	3.898769
H	2.719054	-2.020623	2.910726
H	2.987342	-1.362924	4.536758
C	0.629063	3.296258	-1.231856
H	-0.446060	3.160768	-1.086377
H	0.810282	4.335081	-1.523934
H	0.958879	2.645937	-2.046503
S	1.559053	2.949977	0.313775

SHgSe-
E=-2.48322180
Nimag=-51.53

C	-0.174080	-1.007595	-0.096699
H	-0.736312	-0.582047	-0.931300
H	0.475267	-1.808572	-0.459772
H	-0.865052	-1.409448	0.648718
Hg	1.051533	0.520879	0.825797

Se	2.590507	0.500392	3.066998
C	2.289688	-1.347424	3.737648
H	1.231709	-1.503636	3.953675
H	2.625698	-2.077130	2.999429
H	2.868212	-1.468921	4.656058
C	0.665946	3.297598	-1.343007
H	-0.409386	3.161340	-1.200068
H	0.844634	4.329450	-1.660366
H	1.003328	2.628055	-2.138756
S	1.588455	2.995539	0.216492

SHgTe-
E=-2.45555909
Nimag=-42.39

C	-0.137137	-0.977482	-0.031367
H	0.526624	-1.805894	-0.292068
H	-0.846809	-1.306752	0.732049
H	-0.678529	-0.643670	-0.919979
Hg	1.054626	0.649382	0.775303
Te	2.773407	0.542021	3.123072
C	2.435074	-1.549798	3.683558
H	1.377415	-1.704948	3.896693
H	2.754514	-2.202582	2.871139
H	3.027096	-1.753522	4.577256
C	0.473115	3.410633	-1.342397
H	-0.589913	3.250624	-1.143805
H	0.614740	4.449535	-1.655407
H	0.782329	2.756889	-2.162193
S	1.483597	3.114041	0.162994

SeHgSe-
E=-2.45659179
Nimag=-43.62

C	-0.151785	-0.968541	-0.074213
H	-0.705084	-0.514341	-0.899547
H	0.492242	-1.765349	-0.455785
H	-0.850358	-1.384234	0.656555
Hg	1.085559	0.527494	0.897636
Se	2.597819	0.449726	3.147318
C	2.290301	-1.413862	3.771155
H	1.231231	-1.572831	3.979579
H	2.627625	-2.125752	3.016357
H	2.865535	-1.558743	4.688300
C	0.619740	3.323183	-1.443467
H	-0.443141	3.143112	-1.275727
H	0.762700	4.348230	-1.792511
H	0.996047	2.629021	-2.196382
Se	1.631715	3.111367	0.255577

SeHgTe-
E=-2.42898612
Nimag=-32.43

C	-0.127394	-0.892070	-0.076847
H	-1.097373	-0.413188	-0.233726
H	0.328845	-1.115282	-1.045023
H	-0.257730	-1.816154	0.491685
Hg	1.170705	0.478994	1.008043
Se	2.621897	0.358867	3.258962
C	2.252072	-1.489375	3.895159
H	1.184821	-1.618864	4.080513
H	2.589784	-2.218094	3.156904
H	2.802458	-1.635324	4.827303
C	0.590344	3.323763	-1.604952
H	-0.457280	3.145813	-1.362027
H	0.709463	4.325786	-2.020263
H	0.941326	2.581605	-2.322037
Te	1.798209	3.212005	0.221150

TeHgTe-
E=-2.40147572
Nimag=-8.01

C	-0.081296	-0.859788	-0.042159
H	-0.526728	-0.413515	-0.934508
H	0.530070	-1.721197	-0.324667
H	-0.869501	-1.183606	0.643008
Hg	1.185108	0.605314	0.973962
Te	2.720674	0.426697	3.375395
C	2.297621	-1.653118	3.922930
H	1.226296	-1.780194	4.078263
H	2.645948	-2.317851	3.132443
H	2.834877	-1.864070	4.849142
C	0.489005	3.400021	-1.665815
H	-0.554562	3.217590	-1.409111
H	0.596305	4.397721	-2.094733
H	0.838166	2.651539	-2.377178
Te	1.718163	3.322937	0.147871

Table S5 Cartesian coordinates (Å), energies (E, Hartree), and number of imaginary vibrational frequencies (Nimag) of stationary points, computed at COSMO(water)-ZORA-BLYP-D3(BJ)/TZ2P.

Reactants/Products

S-
E= -0.96422598
Nimag=0

S	0.000000	0.000000	-0.649158
C	0.000000	0.000000	1.222827
H	-0.512737	0.888086	1.609340
H	-0.512737	-0.888086	1.609340
H	1.025474	0.000000	1.609340

Se-
E= -0.93796589
Nimag=0

Se	0.000000	0.000000	-0.764459
C	0.000000	0.000000	1.266257
H	-0.514845	0.891738	1.633297
H	-0.514845	-0.891738	1.633297
H	1.029690	0.000000	1.633297

Te-
E= -0.91028135
Nimag=0

Te	0.000000	0.000000	-0.924295
C	0.000000	0.000000	1.314399
H	-0.516110	0.893928	1.670528
H	-0.516110	-0.893928	1.670528
H	1.032219	0.000000	1.670528

HgS
E= -1.54407727
Nimag=0

C	-0.241186	0.063156	-0.068574
H	-0.195220	-0.879205	-0.620059
H	-1.234060	0.205906	0.364684
H	0.016153	0.900629	-0.721938
Hg	1.184092	-0.014124	1.511818
S	2.809274	-0.073502	3.302788
C	2.741978	-1.862519	3.815111
H	1.744418	-2.126806	4.171691
H	3.028657	-2.514270	2.987351
H	3.460220	-1.976875	4.631258

HgSe
E= -1.51880032
Nimag=0

C	-0.266126	0.067669	-0.099850
H	-0.149106	-0.839101	-0.698353
H	-1.257533	0.101789	0.358173
H	-0.094566	0.956246	-0.712559
Hg	1.199462	0.038642	1.458350
Se	2.939846	0.018325	3.302180
C	2.749355	-1.910159	3.859696
H	1.735389	-2.093575	4.214879
H	2.991797	-2.562801	3.021115
H	3.465810	-2.054643	4.670496

HgTe
E= -1.49363439
Nimag=0

C	-0.316235	0.087434	-0.157559
H	-0.267094	-0.892560	-0.638963
H	-1.307024	0.257032	0.271046
H	-0.063676	0.877612	-0.869287
Hg	1.132506	0.129517	1.435558
Te	2.956556	0.176542	3.441794
C	2.803697	-1.982691	3.910198
H	1.783966	-2.211246	4.217871
H	3.090524	-2.561000	3.032663
H	3.501107	-2.158251	4.730809

Reactant Complexes/Product Complexes

S-+HgS/S-+HgS
E=-2.51947495
Nimag=0

C	-0.281382	-0.250074	-0.619005
H	0.229608	-0.109757	-1.575041
H	-0.554618	-1.299104	-0.484452
H	-1.171521	0.383076	-0.577209
Hg	1.055321	0.375423	0.948974
S	2.521338	0.564265	2.911027
C	2.451030	-1.128914	3.681151
H	1.429219	-1.375172	3.979195
H	2.823310	-1.884887	2.985778
H	3.090322	-1.110395	4.568806
C	0.534578	3.205045	-1.311816
H	-0.512495	2.963232	-1.104594
H	0.581710	4.201458	-1.763108
H	0.921149	2.476100	-2.030902
S	1.537207	3.167390	0.259309

S-+HgSe/Se-+HgS
E=-2.49445388
Nimag=0

C	-0.280024	-0.207194	-0.592219
H	-1.136845	0.471579	-0.589521
H	0.240839	-0.145923	-1.551305
H	-0.604758	-1.232136	-0.399333
Hg	1.088668	0.442075	0.952168
Se	2.614713	0.614040	3.016718
C	2.356394	-1.212612	3.831806
H	1.306080	-1.353494	4.089153
H	2.683017	-1.977661	3.126636
H	2.972047	-1.244836	4.733505
C	0.698629	3.185479	-1.422077

H	-0.357992	3.008570	-1.198614
H	0.795489	4.159253	-1.913157
H	1.040330	2.408609	-2.113102
S	1.710809	3.158106	0.143005

S-+HgTe/Te-+HgS
E=-2.46970597
Nimag=0

C	-0.335346	-0.150924	-0.596070
H	0.147353	-0.059712	-1.572787
H	-0.618725	-1.188644	-0.405697
H	-1.213350	0.499104	-0.552488
Hg	1.078022	0.528022	0.915585
Te	2.757179	0.623195	3.083659
C	2.446504	-1.443469	3.822220
H	1.396298	-1.572879	4.083529
H	2.743329	-2.146794	3.044315
H	3.077765	-1.560883	4.705129
C	0.513653	3.287627	-1.393154
H	-0.530762	3.085183	-1.136575
H	0.574712	4.273348	-1.865809
H	0.845893	2.532262	-2.111916
S	1.580610	3.248207	0.134329

Se-+HgS/S-+HgSe
E=-2.49450016
Nimag=0

C	0.189489	-1.377193	0.636123
H	-0.457904	-1.476072	-0.238190
H	1.018909	-2.086692	0.577869
H	-0.380461	-1.546380	1.553232
Hg	1.018566	0.610382	0.724973
Se	2.695540	0.501271	3.226148
C	2.188517	-1.403773	3.671403
H	1.107822	-1.468742	3.812361
H	2.487875	-2.060397	2.852149
H	2.698674	-1.703468	4.589704
C	0.766735	3.390170	-1.256389
H	-0.314366	3.289013	-1.135442
H	1.007158	4.432091	-1.488099
H	1.106281	2.752132	-2.075681
S	1.648662	2.954156	0.324417

Se-+HgSe/Se-+HgSe
E=-2.46952015
Nimag=0

C	-0.216804	-0.223222	-0.569772
H	-1.086575	0.438698	-0.566902
H	0.311103	-0.141071	-1.523343
H	-0.522675	-1.256492	-0.390646
Hg	1.127660	0.436870	0.994713
Se	2.625751	0.566429	3.086787
C	2.385780	-1.285921	3.849776
H	1.333817	-1.450753	4.085368
H	2.736719	-2.026356	3.130119
H	2.986866	-1.332292	4.760715
C	0.584913	3.224695	-1.442676
H	-0.450195	3.012934	-1.167713
H	0.643371	4.195449	-1.940266
H	0.949978	2.444021	-2.112883
Se	1.727920	3.268752	0.223254

Se-+HgTe/Te-+HgSe
E=-2.44488076
Nimag=0

C	0.195469	-1.359435	0.737419
H	-0.446655	-1.405565	-0.145273
H	0.990655	-2.106712	0.671276
H	-0.391124	-1.519293	1.645942
Hg	1.131790	0.604707	0.882668
Se	2.754707	0.399402	3.357830
C	2.207052	-1.499173	3.779831
H	1.125676	-1.541751	3.923581
H	2.489684	-2.151184	2.951073
H	2.713988	-1.820603	4.692588
C	0.714219	3.462606	-1.553773
H	-0.347291	3.323852	-1.348865
H	0.907386	4.479872	-1.899819
H	1.067051	2.736528	-2.286098
Te	1.853526	3.197776	0.330216

Te-+HgS/S-+HgTe
E=-2.46877980
Nimag=0

C	0.186340	-1.305289	0.554822
H	1.024295	-1.999425	0.452059
H	-0.351373	-1.506916	1.484685
H	-0.486775	-1.391232	-0.301370
Hg	0.991264	0.695432	0.673674
Te	2.828867	0.555041	3.249300
C	2.291758	-1.581386	3.565325
H	1.214484	-1.654461	3.719042
H	2.582501	-2.151460	2.682197
H	2.824885	-1.947587	4.444368
C	0.566836	3.494055	-1.272025
H	-0.504439	3.370965	-1.095831
H	0.774714	4.542088	-1.508135
H	0.875159	2.868318	-2.112986
S	1.537604	3.062817	0.257864

Te-+HgSe/Se-+HgTe
E=-2.44398220
Nimag=0

C	-0.168343	-0.277526	-0.477211
H	-1.033458	0.390287	-0.488127
H	0.365593	-0.211244	-1.428575
H	-0.481699	-1.306379	-0.285520
Hg	1.174318	0.400646	1.087615
Se	2.645353	0.472754	3.208502
C	2.372113	-1.382242	3.956350
H	1.315318	-1.534019	4.179101
H	2.720309	-2.121951	3.234494

H	2.962430	-1.444848	4.873469
C	0.597611	3.163919	-1.575795
H	-0.430807	2.949746	-1.282771
H	0.645836	4.102920	-2.129908
H	0.991898	2.346766	-2.180904
Te	1.840498	3.360370	0.259296

Te-+HgTe/Te-+HgTe
E=-2.41941666
Nimag=0

C	-0.083517	-0.265550	-0.531197
H	0.437526	-0.133031	-1.482980
H	-0.299251	-1.322307	-0.356671
H	-1.007099	0.319318	-0.528006
Hg	1.207615	0.513683	1.052122
Te	2.721512	0.540260	3.352901
C	2.426753	-1.561254	4.002077
H	1.364312	-1.732762	4.175395
H	2.806573	-2.227824	3.227695
H	2.990875	-1.690231	4.927976
C	0.433010	3.257715	-1.575599
H	-0.577449	2.964274	-1.288903
H	0.415396	4.215141	-2.099276
H	0.881002	2.489108	-2.206406
Te	1.663901	3.481110	0.263559

Transition States
SHgS-
E=-2.51663151
Nimag=-60.43

C	-0.196882	-1.018114	-0.105492
H	0.100463	-1.085735	-1.155182
H	-0.059486	-1.980972	0.392252
H	-1.239652	-0.698038	-0.031699
Hg	1.052079	0.482725	0.874494
S	2.562280	0.473296	3.014678
C	2.354832	-1.279740	3.610912
H	1.306393	-1.484412	3.844569
H	2.696290	-1.986901	2.849974
H	2.954126	-1.415292	4.516731
C	0.624434	3.260794	-1.232128
H	-0.442324	3.098708	-1.054594
H	0.776484	4.291741	-1.566975
H	0.963860	2.578928	-2.016751
S	1.597249	2.991492	0.334060

SHgSe-
E=-2.4920517
Nimag=-54.10

C	-0.156860	-0.996672	-0.071111
H	-0.710631	-0.567895	-0.909847
H	0.501587	-1.796789	-0.419748
H	-0.846390	-1.381701	0.684642
Hg	1.081553	0.557692	0.849404
Se	2.619244	0.547385	3.107487
C	2.262672	-1.351366	3.694846
H	1.193319	-1.484237	3.866690
H	2.605471	-2.041506	2.922235
H	2.813531	-1.526291	4.621869
C	0.657718	3.266915	-1.339830
H	-0.408092	3.102404	-1.159120
H	0.803982	4.290989	-1.697618
H	1.002311	2.569346	-2.108165
S	1.630731	3.040207	0.233113

SHgTe-
E=-2.46735309
Nimag=-45.50

C	-0.116484	-1.002682	-0.003579
H	0.572559	-1.798857	-0.297991
H	-0.782933	-1.358492	0.786600
H	-0.694897	-0.661685	-0.865793
Hg	1.069037	0.663891	0.799556
Te	2.765251	0.570144	3.162523
C	2.327527	-1.559890	3.617802
H	1.257093	-1.669101	3.794237
H	2.638402	-2.171713	2.770496
H	2.890422	-1.834079	4.511919
C	0.455192	3.366870	-1.351404
H	-0.598267	3.178640	-1.127154
H	0.566436	4.398250	-1.700813
H	0.781461	2.685929	-2.142190
S	1.498905	3.142738	0.175907

SeHgSe-
E=-2.46753527
Nimag=-48.05

C	-0.124090	-0.950433	-0.055213
H	-0.684281	-0.488262	-0.871597
H	0.531424	-1.736115	-0.440611
H	-0.807177	-1.364816	0.690922
Hg	1.125477	0.572724	0.914585
Se	2.645280	0.490158	3.178543
C	2.254718	-1.413378	3.728711
H	1.183071	-1.530264	3.897827
H	2.585458	-2.094019	2.942547
H	2.802039	-1.616104	4.652228
C	0.605009	3.278706	-1.433871
H	-0.443590	3.065312	-1.220532
H	0.706813	4.293150	-1.826378
H	0.993595	2.559206	-2.156347
Se	1.676399	3.162615	0.274033

SeHgTe-
E=-2.44292210
Nimag=-40.35

C	-0.109910	-0.830992	-0.085236
H	-1.032209	-0.298068	-0.330866
H	0.407920	-1.125124	-1.002439
H	-0.326742	-1.709952	0.526881
Hg	1.205463	0.540361	1.029501
Se	2.661800	0.398761	3.295851

C	2.237693	-1.495410	3.853756
H	1.161463	-1.598353	4.001112
H	2.578441	-2.186889	3.081532
H	2.763362	-1.693616	4.790811
C	0.565561	3.239412	-1.571546
H	-0.465157	3.031264	-1.283032
H	0.637028	4.219291	-2.047270
H	0.937873	2.463509	-2.241028
Te	1.827562	3.274290	0.256817

TeHgTe-
E=-2.41846076
Nimag=-29.88

C	-0.040497	-0.856459	0.002023
H	-0.512821	-0.424993	-0.884019
H	0.596461	-1.700106	-0.278222
H	-0.799315	-1.183122	0.718466
Hg	1.225683	0.674938	0.975231
Te	2.758956	0.470791	3.400295
C	2.242367	-1.643485	3.846142
H	1.160723	-1.725376	3.956681
H	2.591443	-2.271333	3.025856
H	2.742247	-1.919963	4.776472
C	0.478121	3.356375	-1.644699
H	-0.552475	3.177741	-1.336560
H	0.566843	4.330229	-2.130071
H	0.819612	2.565642	-2.313290
Te	1.772798	3.377603	0.160538

Table S6 Cartesian coordinates (Å), energies (E, Hartree), and number of imaginary vibrational frequencies (Nimag) of stationary points, computed at COSMO(diethylether)-ZORA-BLYP-D3(BJ)/TZ2P.

Se^-
E= -0.91441493
Nimag=-0

Se	0.000000	0.000000	-0.765615
C	0.000000	0.000000	1.263851
H	-0.514680	0.891451	1.634484
H	-0.514680	-0.891451	1.634484
H	1.029359	0.000000	1.634484

S^-
E=-0.93914507
Nimag=0

S	0.000000	0.000000	-0.649649
C	0.000000	0.000000	1.219035
H	-0.512507	0.887688	1.610768
H	-0.512507	-0.887688	1.610768
H	1.025013	0.000000	1.610768

HgS
E=-1.54237030
Nimag=0

C	-0.241060	0.064012	-0.068099
H	-0.195606	-0.874094	-0.627032
H	-1.235565	0.202805	0.362936
H	0.012843	0.904926	-0.718589
Hg	1.186344	-0.018421	1.513402
S	2.809119	-0.075741	3.297347
C	2.741635	-1.862256	3.815016
H	1.745561	-2.128265	4.175049
H	3.030885	-2.519577	2.992308
H	3.460170	-1.970999	4.631792

HgSe
E=-1.51741813
Nimag=0

C	-0.016660	0.042150	0.192940
H	-0.263461	-0.991191	-0.062484
H	-0.883676	0.546768	0.626556
H	0.334854	0.581277	-0.690444
Hg	1.557693	0.031088	1.644830
Se	3.430737	0.020995	3.345505
C	2.310290	-0.148479	5.012711
H	1.645639	0.710678	5.103599
H	1.743198	-1.079016	4.987281
H	3.020467	-0.163589	5.841624

ASA plot

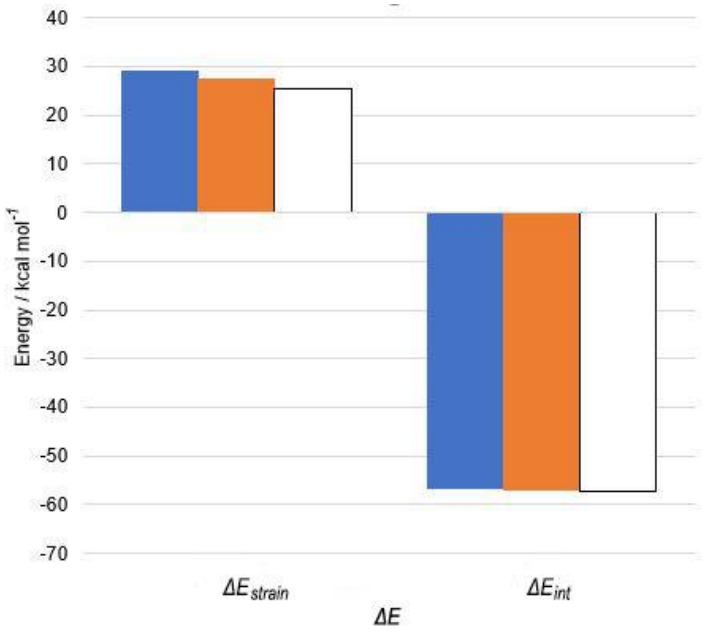

Figure S1. ASA(kcal mol^{-1}) of the TCIs at ZORA-BLYP-D3(BJ)/TZ2P. The fragments are S^- and HgX (X=S (blue), Se (orange), Te (white)).

Reaction profiles in water

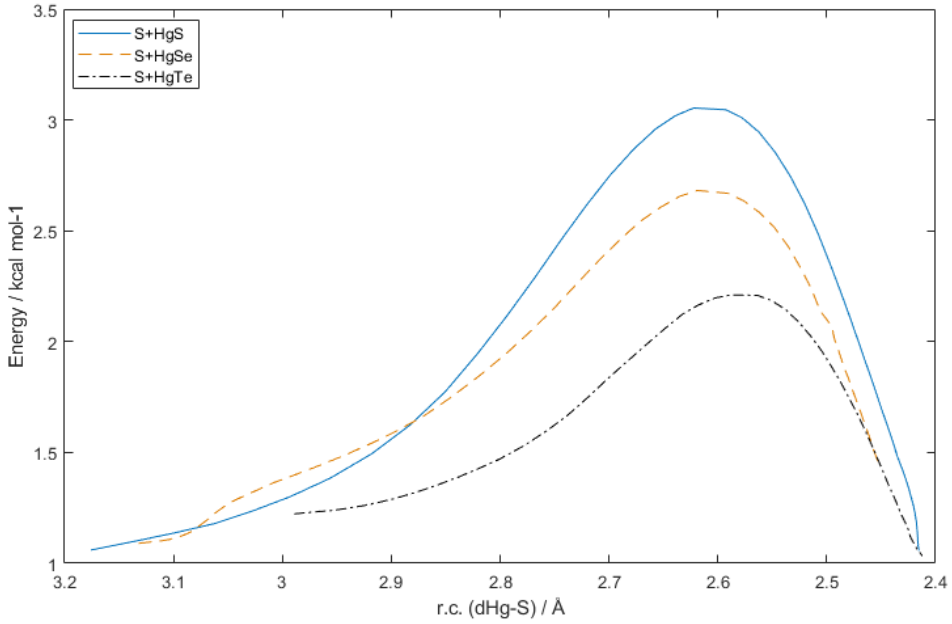

Figure S2. Reaction profiles calculated in water at COSMO-ZORA-OLYP/TZ2P for the reaction S^- + HgX. Energies relative to free reactants of every reaction. The reaction coordinate (r.c.) d_{HgS} is the distance between the sulfur atom of the entering ligand and the mercury atom of the substrate.

Reaction enthalpies and Gibbs free energies

Table S7. Reaction enthalpies and Gibbs free energies for the formation of **S-Hg-S$^-$** computed with the tested functionals combined with TZ2P-ae basis set for all the atoms; energy values are given with respect to the free reactants. Energy values obtained with small-core approximation basis sets, when available, are reported in parentheses. The investigated reaction is: **S$^-$ + Hg-S ⇄ S-Hg-S$^-$.**

	ΔH	ΔG
OLYP	-18.57(-18.13)	-11.63(-11.13)
BLYP	-22.04(-21.72)	-15.5(-15.13)
BLYP-D3(BJ)	-27.16(-26.22)	-21.87(-20.93)
B3LYP	-23.10	-16.25
B3LYP-D3(BJ)	-27.57	-20.24
M06-2X	-26.63	-20.31

Table S8. Gibbs free energies (ΔG) relative to free reactants (kcal mol^{-1}) of the stationary points in gas-phase computed at two different levels of theory, i.e. ZORA-OLYP/TZ2P and ZORA-BLYP-D3(BJ)/TZ2P.

	OLYP			**BLYP-D3(BJ)**	
	R	TCI	P	TCI	P
S$^-$+Hg-S	0.00	-11.13	0.00	-20.93	0.00
S$^-$+Hg-Se	0.00	-12.34	-2.24	-22.34	-2.18
S$^-$+Hg-Te	0.00	-14.82	-8.29	-24.85	-7.05
Se$^-$+Hg-S	0.00	-10.10	2.24	-20.16	2.18
Se$^-$+Hg-Se	0.00	-11.37	0.00	-20.65	0.00
Se$^-$+Hg-Te	0.00	-13.83	-6.05	-23.08	-4.87
Te$^-$+Hg-S	0.00	-6.53	8.29	-17.80	7.05
Te$^-$+Hg-Se	0.00	-7.78	6.05	-18.21	4.87
Te$^-$+Hg-Te	0.00	-10.01	0.00	-20.73	0.00

Table S9. Gibbs free energies relative to free reactants (kcal mol-1) of the stationary points in water computed at two different levels of theory, i.e. COSMO-ZORA-OLYP/TZ2P and COSMO-ZORA-BLYP-D3(BJ)/TZ2P. RC and PC are the reactant complex and the product complex, respectively.

	OLYP			**BLYP-D3(BJ)**			
	R	**TS**	**P**	**RC**	**TS**	**PC**	**P**
S^-+Hg-S	0	13.32	0	2.26	4.09	2.26	0
S^-+Hg-Se	0	14.24	0.93	2.23	3.76	2.5	0.97
S^-+Hg-Te	0	13.06	2.45	1.8	3.51	2.86	2.87
Se^-+Hg-S	0	13.31	-0.93	1.53	2.79	1.26	-0.97
Se^-+Hg-Se	0	11.76	0	1.21	2.36	1.21	0
Se^-+Hg-Te	0	11.62	1.52	0.67	1.96	1.46	1.9
Te^-+Hg-S	0	10.61	-2.45	-0.01	0.64	-1.07	-2.87
Te^-+Hg-Se	0	10.1	-1.52	-0.44	0.06	-1.23	-1.9
Te^-+Hg-Te	0	9.93	0	-1.05	-0.27	-1.05	0

DIPARTIMENTO DI SCIENZE CHIMICHE
Prof. Dr. Laura Orian

UNIVERSITÀ DEGLI STUDI DI PADOVA

via Marzolo 1 - 35131 Padova (Italy)
tel +390498275140
e-mail: laura.orian@unipd.it

Padova, June 8th 2020

To:Prof. Gernot Frenking
Editor
Journal of Computational Chemistry

Re:Revision of Manuscript **JCC-20-0185** 'Chalcogen-mercury bond formation and disruption in model Rabenstein's reactions: a computational analysis', by A. Madabeni, M. Dalla Tiezza, O. B. Folorunsho, P. A. Nogara, M. Bortoli, J. B. T. Rocha and L. Orian.

Dear Prof. Frenking,
thank you for your letter and the Reviewers' last comments on our manuscript.
In detail:

Reviewer 1

We acknowledge once more Reviewer 1 for her/his comments on our manuscript.

Reviewer 2

The comments and criticism by Reviewer 2 have been particularly constructive and we wish to demonstrate once more our appreciation for her/his work. Below are the answers to her/his minor points.

R. *My former point 2 (choice of OLYP for geometry optimizations): The answer given in the "response to referees" is reasonable. I would ask that some of this justification be added to the text (or SI) in a brief manner.*
A.As recommended, we have added the justification in the main text.

R. *My former point 4 (references): "Since the BJ version of Grimme's -D3 correction*

has been used, the corresponding BJ paper should also be cited." This has not yet been done, please add the Becke-Johnson reference.

A. We realize that we misunderstood the recommendation and left the citation we found in the ADF manual. Now three references to the original works by Becke and Johnson have been included.

R. *Gibbs free energy, not "free Gibbs energy" (p. 7, above Table 2).*

A.This has been fixed.

.

All the last changes above described are yellow highlighted in a manuscript file. We look forward to your reply.

Sincerely

Laura Orian

Laura Orian

Dip. Scienze Chimiche Università degli Studi di Padova,
Via Marzolo 1, 35129 Padova, Italy,
Phone : +39 – 0498275140, Fax: +39 – 0498275239,
Email: laura.orian@unipd.it

Chalcogen-mercury bond formation and disruption in model Rabenstein's reactions: a computational analysis

A. Madabeni,[a] M. Dalla Tiezza,[a] O. B. Folorunsho,[b] P. A. Nogara,[a,b] M. Bortoli,[a] J. B. T. Rocha,[b] L. Orian[a*]

[a] Dipartimento di Scienze Chimiche Università degli Studi di Padova Via Marzolo 1 35131 Padova, Italy

[b] Departamento de Bioquímica e Biologia Molecular, Universidade Federal de Santa Maria, Santa Maria RS Brazil

[*] Corresponding author: E-mail: laura.orian@unipd.it

Abstract

Methylmercury is a highly toxic compound and human exposure is mainly related to consumption of polluted fish and seafood. The inactivation of thiol-based enzymes, promoted by the strong affinity binding of electrophilic mercuric ions to thiol and selenol groups of proteins, is likely an important factor explaining its toxicity. A key role is played by the chemistry and reactivity of the mercury-chalcogens bond, particularly Hg-S and Hg-Se, which is the focus of this computational work (level of theory: (COSMO)-ZORA-BLYP-D3(BJ)/TZ2P). We analyze nine ligand-exchange model reactions (the so-called Rabenstein's reactions) involving an entering ligand (methylchalcogenolate) and a substrate (methylchalcogenolatemethylmercury). Trends in reaction and activation energies are discussed and a change in mechanism is reported for all cases when going from gas-phase to water, that is from a single-well PES to a canonical S_N2-like mechanism. The reasons accounting for the biochemically challenging and desired displacement of methylmercury from a seleno/thiol protein can be found already in these model reactions, as can be seen from the similarities of the ligand exchange reactions in solution in thermodynamics and kinetics.

Introduction

Methylmercury (CH_3Hg^+), the methylated form of mercury, is a hazardous neurotoxicant, naturally found in the environment and in food chain.[1,2] Several studies have demonstrated that the CH_3Hg^+ toxicity might involve its interaction with thio- and selenoproteins (due to the high affinity of mercury to sulfur and selenium atoms present in cysteine (Cys) and selenocysteine (Sec) residues, respectively), disrupting their normal function.[3,4]

CH_3Hg^+ might bind to the Cys residue in many proteins and peptides, such as thioredoxin (Trx) and glutathione (GSH), which are the Thioredoxin Reductase (TrxR) and Glutathione

Peroxidase (GPx) substrates, leading to the decrease in the active concentration of these important substrates. In addition, the adducts between Trx and GSH with CH_3Hg^+ (Trx-$HgCH_3$ and GS-$HgCH_3$) might deliver the CH_3Hg^+ moiety to its respective enzymes, inhibiting them.[5,6] As a consequence of these exchange reactions, CH_3Hg^+ can be distributed easily in the organism, according to the Rabenstein's reaction (Eq. 1).

$$RS(e)H + R'S(e)HgCH_3 \rightleftarrows R'S(e)H + RS(e)HgCH_3 \quad (1)$$

The adducts between CH_3Hg^+ and Cys residues are highly stable. However, the S-Hg bond is labile, and in the presence of another thiol (-SH) or selenol (-SeH) groups, exchange reactions may occur. Furthermore, the formation of R-Se-$HgCH_3$ complexes is more favorable than R-S-$HgCH_3$, due to the higher binding affinity between CH_3Hg^+ and –SeH.[4,7–10]

The GPx and TrxR are important selenoenzymes involved in the cell antioxidant defense, cell proliferation, and redox-regulated signaling cascades. GPx is able to reduce hydrogen peroxide and/or organic hydroperoxides to water and/or the corresponding alcohols, respectively,[11,12] while the TrxR can reduce many substrates, such as the oxidized thioredoxin, peroxides, and other disulfide proteins (Scheme 1A and B).[13,14] It is supposed that the GPx and TrxR inhibition by CH_3Hg^+ occurs via the binding of CH_3Hg^+ to the selenium atom of Sec in their active site, leading to the interruption of the catalytic cycle (Scheme 1C and D), and consequently increasing the reactive oxygen species (ROS) levels, causing cell death.[4,15]

However, CH_3Hg^+ mechanism of action is still not well understood and computational methods have been applied to gain insight into methylmercury chemistry with cysteine and selenocysteine. Particularly, Schreckenbach and co-workers carried out an extensive analysis on structural, electronic and thermodynamic properties of methylmercury complexes with cysteine and selenocysteine, but also on the chalcogenophilicity of mercury, assessing that Hg-S bond has a higher bond dissociation energy (BDE) than Hg-Se and Hg-Te in different compounds ranging from small molecules to large complexes. In addition, they investigated *in silico* the thermodynamic feasibility of a degradation mechanism of selenocysteinate complexes of methylmercury[16–20] in order to rationalize mercury-selenium antagonism.[21] The development of an accurate computational method to study CH_3Hg^+ binding, interactions, and reactivity is critical for future work focused on model compounds as well as on systems of increasing complexity up to the thiol- and selenol-based enzymes.

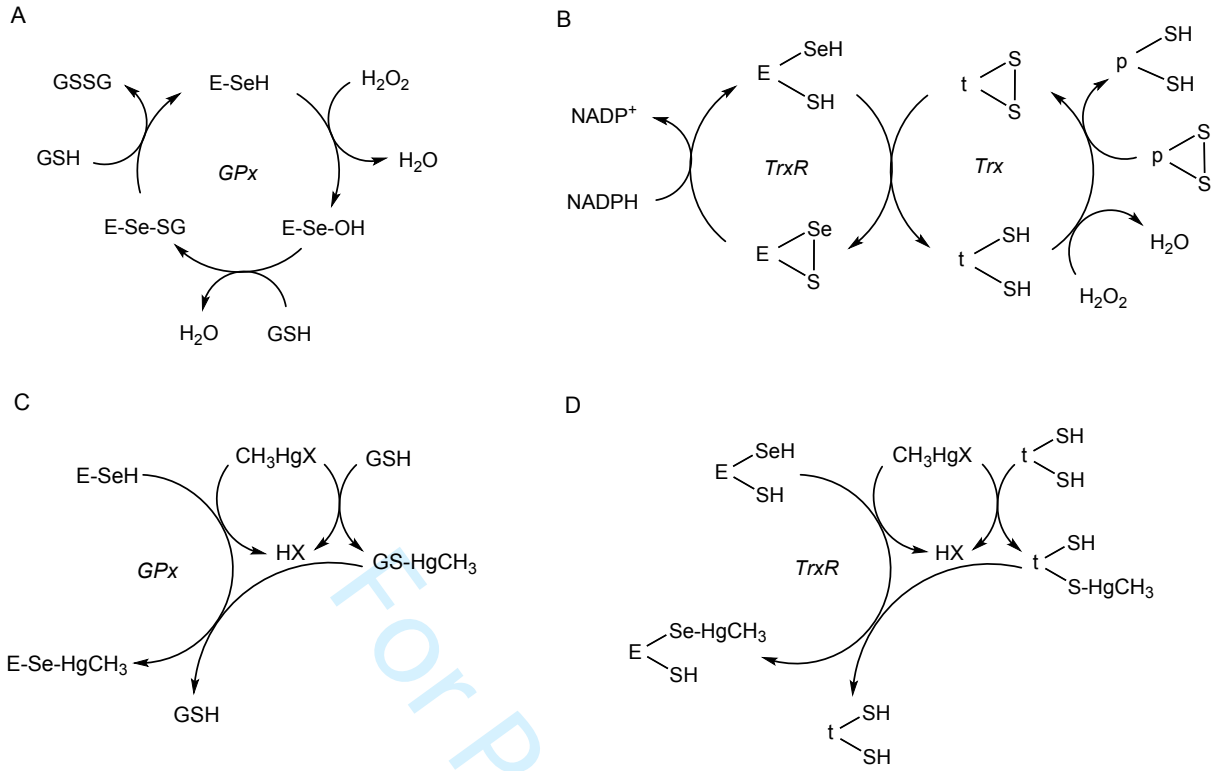

Scheme 1. Catalytic cycle of GPx (A) and TrxR (B) enzymes, and their inhibition by MeHg (C and D, respectively). The enzymes inhibition may occur after the binding of MeHg to the Se atom in Sec residue. E, t, p, and X represent the enzyme, Trx, other disulfide proteins, and chloride/hydroxide anion.

In this work, we have analyzed the reaction of a methylchalcogenolate and a methylchalcogenolatemethylmercury substrate, which affords the formation of a new dinuclear substrate and cleavage of the methylchalcogenolate initially bonded to mercury. These model systems represent the situation in which mercury is bonded to a Cys or a Sec in an enzymatic pocket with the presence of a thiol like glutathione; alternatively, they represent methylmercury bonded to a free cysteine entering in an enzymatic pocket and binding to the active Cys or Sec present in the site. Suitable DFT computational methodologies for structural as well as energetic investigation are discussed and the reaction mechanisms are studied in gas phase as well as in water.

Methods

All Density Functional Theory (DFT) calculations were done with the Amsterdam Density Functional (ADF) program.[22,23] Zeroth-order regular approximation (ZORA) was used in order to include scalar relativistic effects due to the presence of heavy nuclei.[24] Four different functionals were tested, i.e. two GGA (OLYP[25–27], BLYP[26,28]), one hybrid (B3LYP[26,29,30]) and one meta-hybrid (M06-2X[31,32]). In addition, the effect of including Grimme dispersion[33–36] was investigated for BLYP and

B3LYP (BLYP-D3(BJ) and B3LYP-D3(BJ)). The TZ2P basis set, a large uncontracted set of Slater-type orbitals (STOs) of triple-ζ quality, augmented with two sets of polarization functions on each atom was used for every atom. Frozen core approximation was not used in the benchmark calculations, to allow a rigorous comparison among all the chosen functionals (small frozen-core approximation is not available for B3LYP and M06-2X in ADF); in these cases, the all electron basis set is denoted TZ2P-ae. Frequency calculations were performed for all fully optimized geometries. All minima have real frequencies, and all transition states have one imaginary frequency corresponding to the correct normal mode connecting reactants to products. Enthalpies and Gibbs free energies at 298.15 K and 1 atm (ΔG) were calculated from electronic bond energies (ΔE) and our frequency computations using standard statistical-mechanics relationships for an ideal gas, and are reported in Supporting information (Tables S7-S9). Since the trends are identical, in the text we discuss electronic bond energies (ΔE).

For a representative set of reactions, an intrinsic reaction coordinate (IRC) calculation was performed to obtain the reaction profile. The IRC profile is the steepest-descent path from the saddle point (the transition state) to the local minima, representing the reactants and products for the investigated reaction.[37] In these calculations, solvation effects (water) were taken into account using the conductor-like screening model (COSMO)[38], as implemented in ADF. For water, we used an effective radius of 1.93Å for the solvent-excluding surface, derived from the macroscopic density, 78.39 as the relative dielectric constants and the molecular mass. We chose as 0.00 the empirical parameter in the scaling function in the COSMO equation. We used MM3 radii[39] divided by 1.2.

In order to ascertain the correctness of the implicit solvation, analyses were also carried out with an explicit solvent model. The extended tight-binding semi-empirical program GFNn-xTB by Grimme et al.[40,41] was used to build a network of water molecules and subsequently to reoptimize some critical structures with the explicit solvation.

To gain quantitative insight into the stability of a representative set of compounds, we performed activation strain (ASA) and energy decomposition analysis (EDA)[42–44] as implemented in ADF. Using this fragment based approach, according to the ASA scheme, we have decomposed the energy relative to the reactants into *strain*, ΔE_{strain} (i.e. the deformation energy required by the reactants to acquire the structure they have in the compound of interest) and *interaction,* ΔE_{int} *(i.e.* the interaction energy between the deformed reactants) (Eq. 2):

$$\Delta E = \Delta E_{strain} + \Delta E_{int} \quad (2)$$

Within EDA, ΔE_{int} can be written as the sum of *electrostatic interaction* (ΔV_{elstat}), the interaction between Coulomb charge densities, *Pauli repulsion* (ΔE_{Pauli}), related to the repulsive interaction between filled orbitals, *orbital interaction* (ΔE_{oi}) due to stabilizing interactions such as HOMO-LUMO interaction, and *dispersion* (ΔE_{disp}), which takes into account dispersive interactions (Eq. 3):

$$\Delta E_{int} = \Delta V_{elstat} + \Delta E_{Pauli} + \Delta E_{oi} + \Delta E_{disp} \quad (3)$$

To assess the quality of the employed functionals, reference energies were obtained also using the single-reference multiconfiguration domain-based local pair natural orbital coupled cluster singles doubles perturbative triples (DLPNO-CCSD(T)) method, [45] implemented as part of the ORCA computational suite [46,47] . All electron relativistic contracted basis set aug-cc-pVTZ-DK with Douglas−Kroll−Hess (DKH) scalar relativistic Hamiltonians [48] were used.[49]

Results and discussion

The focus of this work is the reaction between a methylchalcogenolate and a methylchalcogenolatemethylmercury substrate in gas phase (GP) and in water (Scheme 2). This ligand-exchange reaction was chosen as a simplified model of the so-called Rabenstein's reaction, involved in the absorption, distribution and excretion of methylmercury from the human body.[4,10] The reaction might proceed either with the formation of a stable three-centers intermediate bismethylchalcogenolatemethylmercurate (TCI) or with a S_N2-like mechanism. These mechanisms closely resemble the reaction between a methylchalcogenolate and a dimethyldichalcogenide, thoroughly investigated by some of us.[50]

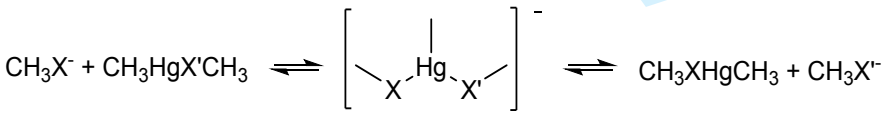

Scheme 2. Model Rabenstein's reaction; X, X' = S, Se, Te.

For clarity, we labelled every compound by the chalcogen(s) and mercury it contains, including the net charge but excluding the methyl groups, i.e. CH_3-S^- is denoted as **S**$^-$, CH_3-Hg-S-CH_3 is **Hg-S**, the three-centers intermediate is **S-Hg-S**$^-$ and so on.

First, we present our benchmark results, carried out on the reaction **S**$^-$ + **Hg-S** in gas-phase: for this reaction, a stable three-center intermediate was easily located at all the tested levels of theory. We focus a) on the different conformers of **S-Hg-S**$^-$; b) on the energetics for the formation of **S-Hg-S**$^-$ described with the different functionals and c) on the relevant geometrical parameters of **Hg-S**. Then,

we extend our investigation to the same reaction including selenium and tellurium. Finally, the results of mechanistic calculations in water are reported and discussed. The effect of the chalcogen and of the solvent were investigated for the influence on both thermodynamics and reaction mechanism

S-Hg-S$^-$ conformers

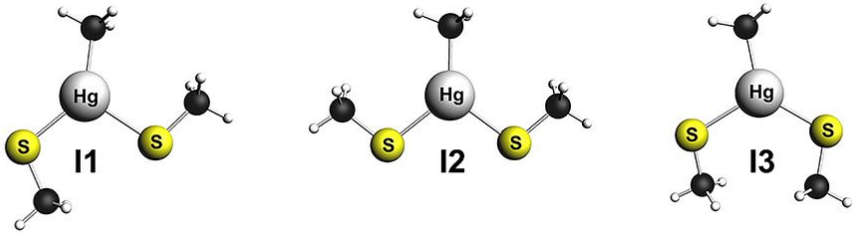

Figure 1. Fully optimized structures of **S-Hg-S**$^-$ denoted isomers **I1**, **I2** and **I3**; level of theory: ZORA-OLYP/TZ2P.

With all the tested functionals, we obtained three conformers for **S-Hg-S**$^-$, as previously reported with cysteinate instead of methylthiolate.[20] Their fully optimized structures are shown in Figure 1, while the energies computed at different levels of theory are reported in Table 1. As a reference, the energies were also calculated at DKH-DLPNO-CCSD(T)/aug-cc-pVTZ-DK level of theory using the OLYP fully optimized structure of each conformer. Since it is well known that geometry is less sensitive to functional/basis sets, we chose OLYP optimization results for our CCSD(T) calculations. In addition, this functional has been benchmarked for organochalcogenides[51] and, by using the same level of theory, it is possible to immediately compare reactivity properties in absence and in presence of methylmercury.

Table 1. Energies (kcal mol^{-1}) relative to the most stable conformer computed with the tested functionals combined with TZ2P-ae basis set for all the atoms; CCSD(T) single point calculations were done using ZORA-OLYP/TZ2P fully optimized geometries. Energy values obtained with small-core TZ2P basis sets, when available, are reported in parentheses.

	OLYP	**BLYP**	**BLYP-D3(BJ)**	**B3LYP**	**B3LYP-D3(BJ)**	**M06-2X**	**CCSD(T)**
I1	0.00 (0.00)	0.00 (0.00)	0.00 (0.00)	0.00	0.00	0.00	0.00
I2	0.98 (0.92)	1.26 (1.24)	2.50 (2.47)	1.56	2.61	3.20	1.82
I3	1.51 (1.49)	1.38 (1.39)	1.01 (1.07)	1.53	1.30	1.14	2.45

In all cases, the conformer **I1** is the most stable one. In general, the relative stability of **I2** and **I3** changes from functional to functional. In agreement with the CCSD(T) trend, pure GGA functionals (OLYP and BLYP) predict **I3** to be the least stable conformer; conversely, the hybrid, the meta-hybrid

and in general the dispersion corrected functionals predict **I2** to be the least stable one. However, BLYP and B3LYP values are definitively too close to establish a meaningful distinction between the stability of **I2** and **I3**. Because, in all cases, the differences in energy between the conformers are within a few kcal mol^{-1}, we chose to retain for further investigation only **I2** conformers, whose intrinsic symmetry reduces the number of structures to calculate when different chalcogens are present on the substrate and on the nucleophile.

A conformational analysis on similar three-center complexes has been done using Stuttgart-Dresden basis set[52] for Hg at B3LYP/SDD (Hg), 6-311+G(p) (S, Se), 6-31+G(p) (H, C, N, O) level of theory by Asaduzzaman et al. with a whole cysteinate/selenocysteinate instead of methylchalcogenolate as nucleophile. A different stability trend was found, i.e. **I2** was identified as the most stable conformer.[20]

Formation energy of S-Hg-S^-

Focusing on **I2**, we computed the formation energies of this **S-Hg-S^-** conformer with all the functionals included in our benchmark (Table 2). At all tested levels of theory, ΔE for the formation of the **S-Hg-S^-** from the free reactants is strongly negative, suggesting highly thermodynamic feasibility. The least and the largest negative values are found with OLYP and B3LYP-D3(BJ), respectively. As expected, the inclusion of dispersion leads to larger (more negative) ΔE values, as can be seen when comparing BLYP vs BLYP-D3(BJ) and B3LYP vs B3LYP-D3(BJ) results. The best agreement with the CCSD(T) value is obtained at ZORA-BLYP-D3(BJ)/TZ2P level of theory. Energies calculated with small-core approximation in the basis set combined to every functional but B3LYP and M06-2X show the same trend and, even in these cases, BLYP-D3(BJ) is the functional affording better agreement with the highly correlated *ab initio* calculations. Gibbs free energies and reaction enthalpies follow the same trend of electronic energies. (Table S7).

Table 2. Formation energies (ΔE) of **S-Hg-S**$^-$ computed with the tested functionals combined with TZ2P-ae basis set for all the atoms and absolute deviations (ΔΔE) of the formation energies (kcal mol^{-1}) with respect to CCSD(T) single point calculations done using ZORA-OLYP/TZ2P fully optimized geometry (ΔE =-27.89). Values obtained with small-core approximation basis set, when available, are reported in parentheses. The investigated reaction is: S^- + Hg-S ⇄ S-Hg-S^-.

Functional	ΔE	ΔΔE
OLYP	-19.49 (-19.04)	8.40 (9.95)
BLYP	-22.93 (-22.60)	4.96 (5.29)
BLYP-D3(BJ)	-28.06 (-27.76)	-0.17 (0.13)
B3LYP	-23.94	3.95
B3LYP-D3(BJ)	-28.48	-0.59
M06-2X	-28.09	-0.20

Structural parameters

The validation of the computed molecular geometries was assessed comparing relevant interatomic distances and angles of the substrate **Hg-S** and MCYSHG10 (Scheme 3) to crystallographic data of similar compounds extracted from the Cambridge Structural Database(CSD).[53] Results are reported in Table 3 and Table 4, respectively.

Table 3. Relevant interatomic distances and angles of **Hg-S** compared to available crystallographic structures (Scheme 3).

	Bond length (Å)			Angles and dihedrals (º)		
	S–Hg	Hg–C	C–S	S–Hg–C	C–S–Hg	C–S–Hg–C
OLYP	2.38	2.11	1.84	178	103	180
BLYP	2.40	2.14	1.86	178	103	180
BLYP-D3(BJ)	2.40	2.14	1.86	179	102	179
B3LYP	2.38	2.12	1.84	178	103	180
B3LYP-D3(BJ)	2.37	2.12	1.84	179	102	179
M06-2X	2.36	2.09	1.83	179	102	180
x-ray (CSD)						
MCYSHG10[a]	2.35	2.10	1.81	178	100	110
PENMHG10[b]	2.38	2.06	1.86	175	107	130
FADVAI[c]	2.35	2.07	1.81	176	100	175

[a] Data taken from Taylor et al. [54]; [b] Data taken from Wong et al[55]; [c] Data taken from Belakhov et al. [56]

Table 4. Relevant interatomic distances and angles computed for MCYSHG10 compared to the crystallographic structure. (Scheme 3)

	Bond length (Å)			Angles and dihedrals (°)		
	S–Hg	Hg–C	C–S	S–Hg–C	C–S–Hg	C–S–Hg–C
OLYP	2.38	2.11	1.84	177	106	159
BLYP	2.41	2.14	1.87	177	105	161
BLYP-D3(BJ)	2.41	2.14	1.86	178	103	176
B3LYP	2.39	2.11	1.84	177	105	163
B3LYP-D3(BJ)	2.38	2.11	1.84	178	104	177
M06-2X	2.37	2.09	1.83	178	103	179
x-ray (CSD)						
MCYSHG10[a]	2.35	2.10	1.81	178	100	110

[a] Data taken from Taylor et al. [54]

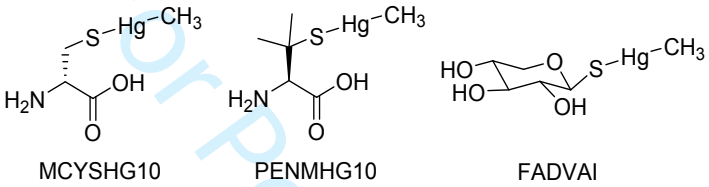

MCYSHG10 PENMHG10 FADVAI

Scheme 3. Mono coordinated methylmercury complexes taken from CSD for structural comparison purposes (Tables 3 and 4)

No structural data exist for our simple methylated structures, so we compared the relevant geometrical parameters of **Hg-S** those of mono coordinated methylmercury complexes sketched in Scheme 3. For **Hg-S**, there is a good agreement between all the calculated and the experimental bond lengths and angles, with little to almost no differences in the parameters computed at different levels of theory. Discrepancies between experimental and *in silico* parameters are of a few hundredths of Å for bond lengths and of a few degrees for angles.

In order to make a more precise comparison between calculated and crystallographic parameters, we chose to optimize the structure of MCYSHG10 (Scheme 3) at all six levels of theory investigated for **Hg-S**. The relevant geometric parameters are reported in Table 4. As precedently stated comparing **Hg-S** computed parameters to the experimental parameters of the compounds in Scheme 3, little to almost no difference is found when using the different levels of theories and all the values are close to the experimental ones. All differences are within a few hundredths of Å for bond lengths and a few degrees for angles. Only C-S-Hg-C dihedral differs from the crystallographic one, likely because of packing effect.

Based on the benchmark results, considering energy and structural results, BLYP-D3(BJ) combined with TZ2P basis sets for all the atoms was chosen for our systematic investigation on model Rabenstein's reactions. M06-2X also performed well in the prediction of both energy values and

structural parameters but was excluded since is computationally more demanding than the dispersion-corrected GGA.

Results obtained with the cheap OLYP functional are also considered to assess the error when tackling these systems with a pure GGA functional. Both OLYP and BLYP-D3(BJ) have been employed successfully for mechanistic studies involving methyl- and aryl-chalcogenides.[50,57–59]

Mechanism of the Rabenstein's reactions

The gas-phase mechanism of the Rabenstein's reactions was investigated changing S, Se, Te on the entering ligand and on the substrate; overall nine reactions were considered. The results are shown in Table 5.

Table 5. Electronic energies (ΔE) relative to reactants (kcal mol^{-1}) of the stationary points in gas-phase computed at three different levels of theory, i.e. ZORA-OLYP/TZ2P, ZORA-BLYP-D3(BJ)/TZ2P and CCSD(T) single point calculations, which were done using ZORA-OLYP/TZ2P fully optimized geometries.

	OLYP		**BLYP-D3(BJ)**		**CCSD(T)**	
	TCI	P	TCI	P	TCI	P
S$^-$+Hg-S	-19.04	0.00	-27.76	0.00	-27.89	0.00
S$^-$+Hg-Se	-20.53	-2.71	-29.35	-2.64	-29.64	-2.71
S$^-$+Hg-Te	-23.22	-8.69	-31.97	-8.11	-32.48	-8.66
Se$^-$+Hg-S	-17.82	2.71	-26.71	2.64	-26.93	2.71
Se$^-$+Hg-Se	- 19.26	0.00	-28.16	0.00	-28.64	0.00
Se$^-$+Hg-Te	- 21.93	-5.98	-30.76	-5.47	-31.46	-5.95
Te$^-$+Hg-S	-14.53	8.69	-23.86	8.11	-23.82	8.66
Te$^-$+Hg-Se	-15.95	5.98	-25.29	5.47	-25.51	5.95
Te$^-$+Hg-Te	-18.48	0.00	-27.80	0.00	-28.23	0.00

We chose to compare the trends obtained with OLYP functional, which well described the energetics for the reaction of a methylchalcogenolate and a dimethyldichalcogenide substrate[50] and BLYP-D3(BJ), which best reproduced the CCSD(T) results in the case of **S$^-$+Hg-S**. At ZORA-OLYP/TZ2P level, all the reactions proceed via a single-well mechanism without any appreciable barrier for the formation of a three-center intermediate (TCI) from the reactants and from the TCI to the products. This is in agreement with typical S_N2 reactions involving heavy central atoms.[60] The inclusion of dispersion (BLYP-D3(BJ)) leads to slightly asymmetric TCIs even when two equal chalcogenolates are bonded to the methylmercury moiety. By analogy with the trichalcogenides[50], this suggests the

existence of two equivalent structures near the bottom of the potential energy surface, separated by a low-energy transition state. Thus, the reaction energy profile is likely a flattened double well curve, but the complete characterization of these low-energy transition states and the exploration of the whole potential energy surface around TCI weren't pursued since they would not provide additional useful information on the reaction. In all cases, the TCI is highly stabilized with respect to the free reactants. As in the model **S**$^-$ +**Hg-S** reaction used in the benchmark, ZORA-BLYP-D3(BJ)/TZ2P results nicely agree with CCSD(T) calculations performed on OLYP fully optimized geometries also when changing the chalcogen from S, to Se and Te in the entering ligand as well as in the substrate. Importantly, ZORA-OLYP/TZ2P values show the same trend, but their high deviation from the *ab initio* results for the TCIs formation energy lead us to consider in the discussion mainly the energetics computed with the dispersion corrected functional.

From the data of Table 5, the effect of changing chalcogen in the entering ligand can be seen. Particularly, when going from **S**$^-$, to **Se**$^-$ and to **Te**$^-$, the TCIs become progressively less stable and the effect is more remarkable when passing from Se to Te. This is likely due to the stabilization of the negative charge, which becomes more diffuse on the entering ligand when increasing the size of the chalcogen, weakening the electrostatic contribution to the formation of the TCI. The same trend is observed for the overall reaction energy, which becomes less and less negative when going from S$^-$ to Se$^-$ and Te$^-$. Comparing the entering ligand and the leaving methylchalcogenolate it can be seen that the stabilization of the negative charge which, in gas phase, is energetically favored on the heavier chalcogens plays a key role in establishing the trend in these processes. The trends in thermodynamics, in fact, are those expected considering nucleophilicity and leaving group capabilities in gas phase. Particularly, the energetics of the reactions changes significantly, since **S**$^-$ + **Hg-X** is favored in all cases while **Te**$^-$ +**Hg-X** is unfavored in all cases. An intermediate situation is found with the **Hg-Se** substrate: the reaction with **S**$^-$ has a negative ΔE, while the reaction with **Te**$^-$ has a positive ΔE. The presence of a different chalcogen in the substrate leads to a stabilization of the TCIs, which increases by approximately 2 kcal mol^{-1} when going from **Hg-S** to **Hg-Se** and **Hg-Te**. Also, the overall reaction becomes more favorable for the same entering ligand when a substrate with a heavier chalcogen is involved. The explanation based on charge distribution effects nicely fits these results too, since in the TCIs/products the charge is more diffuse when a heavier chalcogen is present/cleaved on/from the substrate, leading to larger stabilization. Gibbs free energies obtained at both levels of theory show the same trends. (Table S8).

Notably, all these trends do not depend on the level of theory and, for what concerns the overall reaction energy trends, there is a good agreement between all the three tested methods. Even if OLYP,

the cheapest functional used in this work, leads to significantly underestimated (about 10 kcal mol^{-1}) TCI formation energies, it correctly predicts trends in agreement with more sophisticated computational approaches.

Table 6. ASA and EDA (kcal mol^{-1}) of the TCIs at ZORA-BLYP-D3(BJ)/TZ2P. The fragments are **S$^-$** and **Hg-X**.

	S-Hg-S$^-$	**S-Hg-Se$^-$**	**S-Hg-Te$^-$**
ΔE	-27.76	-29.35	-31.97
ΔE_{strain}	28.97	27.54	25.42
ΔE_{int}	-56.73	-56.89	-57.39
ΔE_{elstat}	-122.47	-123.45	-124.58
ΔE_{Pauli}	129.80	132.09	134.73
ΔE_{oi}	-59.22	-60.58	-62.43
ΔE_{disp}	-4.84	-4.95	-5.11

In order to obtain a quantitative insight into the TCI stability with respect to the free reactants we performed ASA and EDA according to Eqs. 2 and 3, choosing **S$^-$** and **Hg-X** as fragments, i.e. focusing on the formation energies of **S-Hg-S$^-$**, **S-Hg-Se$^-$**, **S-Hg-Te$^-$** with respect to different substrates (**Hg-S**, **Hg-Se**, **Hg-Te**), and the results are shown in Table 6 and Figure S1.

For the attack of S$^-$ to HgX, little to almost no difference is present in the interaction energy, which remains almost constant for the three intermediates. The formation energy of the three-center intermediate becomes more negative when increasing the size of the chalcogen on the substrate principally because of a net decrease of the strain energy when going from **Hg-S** to **Hg-Se** to **Hg-Te**, because the bonds become more and more soft. The stability of the TCI with respect to different substrates appears to be *strain-controlled*, while the changes in electrostatic interaction, Pauli repulsion and orbital interaction compensate each other leading to no significant change to the overall interaction energy. Also, dispersion variations play a marginal role and do not vary appreciably.

We extended our investigation on the model Rabenstein's reactions carrying out mechanistic calculations in water. Again, both ZORA-OLYP/TZ2P and ZORA-BLYP-D3(BJ)/TZ2P were used and the results are shown in Table 7. Gibbs free energies follow essentially the same behavior (Table S9).

Table 7. Electronic energies (ΔE) relative to reactants (kcal mol^{-1}) of the stationary points in water computed at two different levels of theory, i.e. COSMO-ZORA-OLYP/TZ2P and COSMO-ZORA-BLYP-D3(BJ)/TZ2P. Activation energies relative to reactant complexes (RC), when present, are shown in parentheses. PC refers to product complexes.

	OLYP		BLYP-D3(BJ)			
	TS	P	RC	TS	PC	P
S^-+Hg-S	4.27	0.00	-7.01	-5.23(1.78)	-7.01	0.00
S^-+Hg-Se	3.93	0.56	-7.17	-5.66(1.51)	-7.20	0.62
S^-+Hg-Te	3.50	1.47	-7.43	-5.96(1.47)	-6.86	2.19
Se^-+Hg-S	3.37	-0.56	-7.82	-6.28(1.54)	-7.79	-0.62
Se^-+Hg-Se	3.00	0.00	-8.00	-6.76(1.24)	-8.00	0.00
Se^-+Hg-Te	2.54	0.91	-8.33	-7.10(1.23)	-7.77	1.58
Te^-+Hg-S	2.03	-1.47	-9.05	-8.15(0.90)	-9.62	-2.19
Te^-+Hg-Se	1.63	-0.91	-9.35	-8.68(0.67)	-9.91	-1.58
Te^-+Hg-Te	1.10	0.00	-9.73	-9.13(0.60)	-9.73	0.00

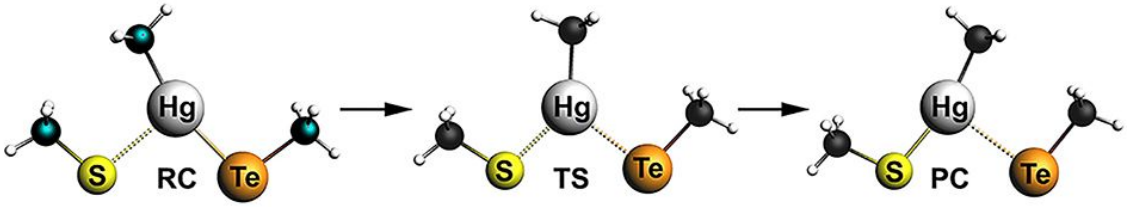

Figure 2. Fully optimized structures of reactant complex (RC), transition state (TS) and product complex (PC) for the reaction **S^-+Hg-Te**, computed at COSMO-ZORA-BLYP-D3(BJ)/TZ2P level of theory.

Moving from gas-phase to solvent, both functionals predict a change in mechanism. While in gas-phase the reaction proceeds with a single-well profile, in water at COSMO-ZORA-OLYP/TZ2P level of theory, a unimodal potential energy surface is found, suggesting a S_N2-like mechanism (Figure S2). The three-center species identified as a minimum on the PES in gas-phase, converged as transition states at higher energy with respect to the free reactants in water.

No stable three-center intermediates were located even when adding dispersion at COSMO-ZORA-BLYP-D3(BJ)/TZ2P. In this latter case, the reaction profile is a true double-well with a transition state at negative energies with respect to the free reactants, connecting weakly bonded reactant complexes to product complexes, both stabilized with respect to the free reactants and products (Figure 2) The shift downward of the BLYP-D3(BJ) PES with respect to the OLYP PES suggests also at this level of theory a S_N2-like mechanism. (Figure 3)

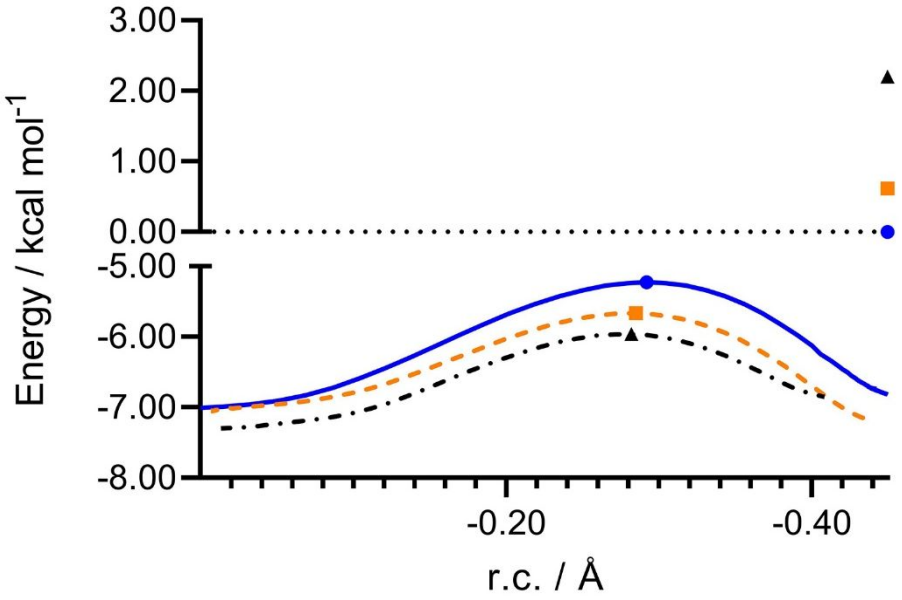

Figure 3. Reaction profiles for S^-+**Hg-X** (X=S (blue solid line), Se (orange dashed line), Te (black dash-dotted line)) in water, computed at COSMO-ZORA-BLYP-D3(BJ)/TZ2P. The reaction coordinate (r.c.) is defined as r.c. = (d_{Hg-S} - d_{Hg-S}^0), where d_{Hg-S}^0 refers to the Hg-S bond length in the reactant complex of each reaction. Filled dots (X=S (circles), Se (squares), Te (triangles)) represent the position of the transition states and the energy value of the free products for each reaction. Since the product complexes are much more stabilized than the free products, the energy axis has been cut and the free products appear on the upper right corner of the graph.

Both OLYP and BLYP-D3(BJ) predict an inversion in the overall reaction thermodynamic trends, with respect to the gas phase. This is in agreement with the known concept of polar solvent stabilizing better species where the charge is more localized.[61,62] The destabilization of the three-center intermediate, where the charge is more diffuse compared to the free reactants, is strong enough to turn the stable gas phase TCI into a transition state.

Changing the chalcogen on the entering ligand from S, to Se and to Te leads to progressively stabilized products. This can make the ligand exchange reaction turn from unfavored (S^- + **Hg-Se**) to favored (Te^- + **Hg-Se**) with implications in methylmercury biochemistry. Conversely, changing the chalcogen on the substrate from S, to Se and to Te leads to an increase of the reaction energy, which becomes more positive as the chalcogen becomes heavier. A similar inversion in the thermodynamic trends was theoretically investigated by Riccardi et al. who observed that in gas-phase Hg^{2+} prefers hard ligands, while in water the expected HSAB theory trend is recovered, with Hg^{2+} preferring softer ligands.[63]

All the activation energies computed at COSMO-ZORA/BLYP-D3(BJ)/TZ2P are below 2 kcal mol^{-1}, and the differences between them are too small to establish some meaningful distinction, particularly when S and Se are involved. All the values are close to those computed for S^- + **Hg-S**,

which has been experimentally described, with different thiolates, as an almost diffusion-controlled associative ligand exchange reaction. [8]

The TCIs have also been optimized in explicit solvent without finding substantial differences from the continuum solvation description. After creating a box of water molecules, the TCIs have been inserted and the system has been optimized without any potential or geometrical constraints. As obtained with the COSMO model, the system evolves to a natural Hg-X bond disruption (see Supporting information).

Conclusions

In this work, we have employed a scalar relativistic DFT approach to analyze ligand-exchange model reactions, known as Rabenstein's reactions, involving an entering ligand (methylchalcogenolate) and a substrate (methylchalcogenolatemethylmercury). The major outcome of our preliminary benchmark, carried out including the zeroth order regular approximation (ZORA) for the relativistic effects and Slater type all electron basis sets of triple-ζ quality with two polarization functions (TZ2P ae), is that BLYP-D3(BJ), that is the method we recommend for these and analogous molecular systems, performs rather well in describing the relevant structural features as well as the energetics. Another functional which provides results in nice agreement with crystallographic structures and CCSD(T) calculations is M06-2X. Importantly, the pure GGA OLYP works well for geometry optimizations, and, despite energies show deviations of almost 10 kcal mol^{-1} from CCSD(T) reference values, it reproduces correctly the trends observed when changing the chalcogens.

The reaction profile in gas phase shows a single minimum, which corresponds to a stable three-center intermediate (TCI). The stability of the TCI increases with increasing chalcogen size in the substrate and decreases when increasing the chalcogen size in the entering ligand. The extent of charge diffusion explains these trends and the trend in the overall reaction energy which becomes less and less negative when going from $\mathbf{S^-}$ to $\mathbf{Se^-}$ and $\mathbf{Te^-}$. Notably, it emerges that $\mathbf{S^-}$ + **Hg-X** is favored in all cases while $\mathbf{Te^-}$ +**Hg-X** is unfavored in all cases; when the substrate is **Hg-Se**, the reaction with $\mathbf{S^-}$ has a negative ΔE, while the reaction with $\mathbf{Te^-}$ has a positive ΔE.

When modeling the Rabenstein's reactions in water, using COSMO continuum description of the condensed phase, a change in mechanism is observed in all cases. The profiles computed at COSMO-ZORA/BLYP-D3(BJ)/TZ2P are characterized by the presence of reactant and product complexes, stabilized with respect to the free reactants and products, respectively, connected by a transition state.

The change in mechanism from gas to condensed phase is analogous to those reported for S_N2 reactions[60] at P[64], or at X (X=S, Se),[50] and is here described for a ligand exchange reaction at Hg. The profiles involving methylthiolate as entering ligand, which are the most interesting from a biochemical point of view, show that **S**$^-$ + **Hg-S** and **S**$^-$ + **Hg-Se** have rather similar energetics, characterized by low activation and neutral reaction energies. In a hydrophobic environment, such as an enzymatic cavity where water is not allowed into, an intermediate regime between the gas phase and the water mechanism is expected, as extensively investigated for reactions with a similar behavior.[64] For the specific case of **S**$^-$ + **Hg-Se**, the products lay at -0.14 kcal mol^{-1} with respect to the free reactants, showing an almost neutral, even if slightly favorite, reaction energy. (Table S6) We must stress that substituents and weak interactions inside the enzymatic cavity may play an important role in tuning the displacement of methylmercury bonded to a selenoprotein by a thiolate. This analysis paves the way for mechanistic investigations of methylmercury bonding to thiol- and seleno-targets of increasing complexity, with the ambitious goal of understanding its toxicology *in silico* and rationally designing paths of detoxification.

Conflict of interest

There are no conflicts to declare.

Acknowledgements

This research was funded by the Università degli Studi di Padova, thanks to the P-DiSC (BIRD2018-UNIPD) project MAD^{3}S (Modeling Antioxidant Drugs: Design and Development of computer-aided molecular Systems); P.I. L.O. All the calculations were carried out on Galileo (CINECA: Casalecchio di Reno, Italy) thanks to the ISCRA Grant MEMES (MEthylMErcury and Selenoproteins), P.I.: L.O. M.D.T. is grateful to Fondazione CARIPARO forfinancial support (PhD grant). J.R., O.F., and P.N. would like to thank the financial support by Coordination for Improvement of Higher Education Personnel CAPES/PROEX (n° 23038.005848/2018-31; n°0737/2018; n°88882.182123/2018-01; nº 88887.354370/2019-00), the CAPES/PrInt – Institutional Internationalization Project (nº 88887.374997/2019-00), the National Council for Scientific and Technological Development (CNPq), and the Rio Grande do Sul Foundation for Research Support (FAPERGS). The authors are grateful to the anonymous referees for their insightful suggestions, which have contributed to improve the quality of this work.

References

[1] M. R. Karagas, A. L. Choi, E. Oken, M. Horvat, R. Schoeny, E. Kamai, W. Cowell, P. Grandjean, S. Korrick, *Environ. Health Perspect.* **2012**, *120*, 799–806.

[2] Y. S. Hong, Y. M. Kim, K. E. Lee, *J. Prev. Med. Public Heal.* **2012**, *45*, 353–363.

[3] J. L. Franco, T. Posser, P. R. Dunkley, P. W. Dickson, J. J. Mattos, R. Martins, A. C. D. Bainy, M. R. Marques, A. L. Dafre, M. Farina, *Free Radic. Biol. Med.* **2009**, *47*, 449–457.

[4] P. A. Nogara, C. S. Oliveira, G. L. Schmitz, P. C. Piquini, M. Farina, M. Aschner, J. B. T. Rocha, *Biochim. Biophys. Acta - Gen. Subj.* **2019**, *1863*, 129284.

[5] V. Branco, C. Carvalho, *Biochim. Biophys. Acta - Gen. Subj.* **2019**, *1863*, 129255.

[6] M. Farina, M. Aschner, *Biochim. Biophys. Acta - Gen. Subj.* **2019**, *1863*, 129285.

[7] D. L. Rabenstein, C. A. Evans, *Bioinorg. Chem.* **1978**, *8*, 107–114.

[8] D. L. Rabenstein, R. S. Reid, *Inorg. Chem.* **1984**, *23*, 1246–1250.

[9] D. L. Rabenstein, *J. Chem. Educ.* **1978**, *55*, 292–296.

[10] A. P. Arnold, K. S. Tan, D. L. Rabenstein, *Inorg. Chem.* **1986**, *25*, 2433–2437.

[11] M. Bortoli, M. Torsello, F. M. Bickelhaupt, L. Orian, *ChemPhysChem* **2017**, *18*, 2990–2998.

[12] L. Orian, P. Mauri, A. Roveri, S. Toppo, L. Benazzi, V. Bosello-Travain, A. De Palma, M. Maiorino, G. Miotto, M. Zaccarin, et al., *Free Radic. Biol. Med.* **2015**, *87*, 1–14.

[13] R. B. Flohé, M. Maiorino, *Biochim. Biophys. Acta - Gen. Subj.* **2013**, *1830*, 3289–3303.

[14] E. S. J. Arnér, *Biochim. Biophys. Acta - Gen. Subj.* **2009**, *1790*, 495–526.

[15] H. Steinbrenner, H. Sies, *Biochim. Biophys. Acta - Gen. Subj.* **2009**, *1790*, 1478–1485.

[16] J. M. Parks, J. C. Smith, *Methods in Enzymology*, Elsevier Inc., **2016**, p 103-122

[17] A. M. Asaduzzaman, M. A. K. Khan, G. Schreckenbach, F. Wang, *Inorg. Chem.* **2010**, *49*, 870–878.

[18] A. Asaduzzaman, D. Riccardi, A. T. Afaneh, S. J. Cooper, J. C. Smith, F. Wang, J. M. Parks, G. Schreckenbach, *Acc. Chem. Res.* **2019**, *52*, 379–388.

[19] A. M. Asaduzzaman, G. Schreckenbach, *Inorg. Chem.* **2011**, *50*, 3791–3798.

[20] A. M. Asaduzzaman, G. Schreckenbach, *Inorg. Chem.* **2011**, *50*, 2366–2372.

[21] M. A. K. Khan, F. Wang, *Environ. Toxicol. Chem.* **2009**, *28*, 1567–1577.

[22] G. te Velde, F. M. Bickelhaupt, E. J. Baerends, C. Fonseca Guerra, S. J. A. van Gisbergen, J. G. Snijders, T. Ziegler, *J. Comput. Chem.* **2001**, *22*, 931–967.

[23] E. J. Baerends, T. Ziegler, A. J. Atkins, J. Autschbach, D. Bashford, O. Baseggio, A. Bérces, F. M. Bickelhaupt, C. Bo, P. M. Boerritger, L. Cavallo, C. Daul, D. P. Chong, D. V Chulhai, L. Deng, R. M. Dickson, J. M. Dieterich, D. E. Ellis, M. van Faassen, A. Ghysels, A. Giammona, S. J. A. van Gisbergen, A. Goez, A. W. Götz, S. Gusarov, F. E. Harris, P. van den Hoek, Z. Hu, C. R. Jacob, H. Jacobsen, L. Jensen, L. Joubert, J. W. Kaminski, G. van Kessel, C. König, F. Kootstra, A. Kovalenko, M. Krykunov, E. van Lenthe, D. A. McCormack, A. Michalak, M. Mitoraj, S. M. Morton, J. Neugebauer, V. P. Nicu, L. Noodleman, V. P. Osinga, S. Patchkovskii, M. Pavanello, C. A. Peeples, P. H. T. Philipsen, D. Post, C. C. Pye, H. Ramanantoanina, P. Ramos, W. Ravenek, J. I. Rodríguez, P. Ros, R. Rüger, P. R. T. Schipper, D. Schlüns, H. van Schoot, G. Schreckenbach, J. S. Seldenthuis, M. Seth, J. G. Snijders, M. Solà, S. M., M. Swart, D. Swerhone, G. te Velde, V. Tognetti, P. Vernooijs, L. Versluis, L. Visscher, O. Visser, F. Wang, T. A. Wesolowski, E. M. van Wezenbeek, G. Wiesenekker, S. K. Wolff, T. K. Woo and A. L. Yakovlev, ADF2018, SCM, Theoretical Chemistry, Vrije Universiteit, Amsterdam, The Netherlands.

[24] E. Van Lenthe, E. J. Baerends, J. G. Snijders, *J. Chem. Phys.* **1994**, *101*, 9783–9792.

[25] N. C. Handy, A. J. Cohen, *Mol. Phys.* **2001**, *99*, 403–412.

[26] C. Lee, W. Yang, R. G. Parr, *Phys. Rev. B* **1988**, *37*, 785–789.

[27] B. G. Johnson, P. M. W. Gill, J. A. Pople, *J. Chem. Phys.* **1993**, *98*, 5612–5626.

[28] A. D. Becke, *Phys. Rev. A* **1988**, *38*, 3098–3100.

[29] A. D. Becke, *J. Chem. Phys.* **1993**, *98*, 5648–5652.

[30] P. J. Stephens, F. J. Devlin, C. F. Chabalowski, M. J. Frisch, *J. Phys. Chem.* **1994**, *98*, 11623–11627.

[31] Y. Zhao, D. G. Truhlar, *Theor. Chem. Acc.* **2008**, *120*, 215–241.

[32] Y. Zhao, D. G. Truhlar, *J. Chem. Phys.* **2006**, *125*, 194101.

[33] S. Grimme, S. Ehrlich, L. Goerigk, *J. Comput. Chem.* **2011**, *32*, 1456–1465.

[34] A. D. Becke, E. R. Johnson, *J. Chem. Phys.* **2005**, *123*, 154101.

[35] E. R. Johnson, A. D. Becke, *J. Chem. Phys.* **2005**, *123*, 024101.

[36] A. D. Becke, E. R. Johnson, *J. Chem. Phys.* **2005**, *122*, 154104.

[37] L. Deng, T. Ziegler, *Int. J. Quantum Chem.* **1994**, *52*, 731–765.

[38] A. Klamt, G. Schüürmann, *J. Chem. Soc. Perkin Trans. 2* **1993**, 799–805.

[39] N. L. Allinger, X. Zhou, J. Bergsma, *J. Mol. Struct. THEOCHEM* **1994**, *312*, 69–83.

[40] S. Grimme, C. Bannwarth, P. Shushkov, *J. Chem. Theory Comput.* **2017**, *13*, 1989–2009.

[41] C. Bannwarth, S. Ehlert, S. Grimme, *J. Chem. Theory Comput.* **2019**, *15*, 1652–1671.

[42] F. M. Bickelhaupt, E. J. Baerends, *Rev. Comput. Chem.* **2000**, *15*, 1–86.

[43] F. M. Bickelhaupt, K. N. Houk, *Angew. Chemie - Int. Ed.* **2017**, *56*, 10070–10086.

[44] T. Ziegler, A. Rauk, *Inorg. Chem.* **1979**, *18*, 1558–1565.

[45] D. G. Liakos, Y. Guo, F. Neese, *J. Phys. Chem. A* **2020**, *124*, 90–100.

[46] F. Neese, *Wiley Interdiscip. Rev. Comput. Mol. Sci.* **2012**, *2*, 73–78.

[47] F. Neese, *Wiley Interdiscip. Rev. Comput. Mol. Sci.* **2018**, *8*, e1327

[48] F. Neese, A. Wolf, T. Fleig, M. Reiher, B. A. Hess, *J. Chem. Phys.* **2005**, *122*, 204107

[49] D. A. Pantazis, F. Neese, *Wiley Interdiscip. Rev. Comput. Mol. Sci.* **2014**, *4*, 363–374.

[50] M. Bortoli, L. P. Wolters, L. Orian, F. M. Bickelhaupt, *J. Chem. Theory Comput.* **2016**, *12*, 2752–2761.

[51] F. Zaccaria, L. P. Wolters, C. Fonseca Guerra, L. Orian, *J. Comput. Chem.* **2016**, *37*, 1672–1680.

[52] D. Figgen, G. Rauhat, M. Dolg, H. Stoll, *Chem. Phys.* **2005**, *311*, 227.

[53] C. R. Groom, I. J. Bruno, M. P. Lightfoot, S. C. Ward, *Acta Crystallogr. Sect. B Struct. Sci. Cryst. Eng. Mater.* **2016**, *72*, 171–179.

[54] N. . Taylor, Y. S. Wong, P. C. Chieh, A. J. Carty, *J.C.S. Dalt. Trans* **1975**, *5*, 438–442.

[55] Y. S. Wong, A. J. Carty, C. Chieh, *J.C.S. Dalt. Trans* **1977**, *19*, 1801–1808.

[56] V. Belakhov, E. Dor, J. Hershenhorn, M. Botoshansky, T. Bravman, M. Kolog, Y. Shoham, G. Shoham, T. Baasov, *Isr. J. Chem.* **2000**, *40*, 177–188.

[57] M. Bortoli, F. Zaccaria, M. D. Tiezza, M. Bruschi, C. F. Guerra, F. Matthias Bickelhaupt, L. Orian, *Phys. Chem. Chem. Phys.* **2018**, *20*, 20874–20885.

[58] M. Bortoli, S. M. Ahmad, T. A. Hamlin, F. M. Bickelhaupt, L. Orian, *Phys. Chem. Chem. Phys.* **2018**, *20*, 27592–27599.

[59] M. Bortoli, M. Bruschi, M. Swart, L. Orian, *New J. Chem.* **2020**, *44*, 6724-6731

[60] T. A. Hamlin, M. Swart, F. M. Bickelhaupt, *ChemPhysChem* **2018**, *19*, 1315–1330.

[61] J. K. Laerdahl, E. Uggerud, *Int. J. Mass Spectrom.* **2002**, *214*, 277–314.

[62] G. Schreckenbach, *Chem. - A Eur. J.* **2017**, *23*, 3797–3803.

[63] D. Riccardi, H. B. Guo, J. M. Parks, B. Gu, A. O. Summers, S. M. Miller, L. Liang, J. C. Smith, *J. Phys. Chem. Lett.* **2013**, *4*, 2317–2322.

[64] T. A. Hamlin, B. van Beek, L. P. Wolters, F. M. Bickelhaupt, *Chem. - A Eur. J.* **2018**, *24*, 5927–5938.

Chalcogen-mercury bond formation and disruption in model Rabenstein's reactions: a computational analysis

A. Madabeni,[a] M. Dalla Tiezza,[a] O. B. Folorunsho,[b] P. A. Nogara,[a,b] M. Bortoli,[a] J. B. T. Rocha,[b] L. Orian[a*]

[a] Dipartimento di Scienze Chimiche Università degli Studi di Padova Via Marzolo 1 35131 Padova, Italy

[b] Departamento de Bioquímica e Biologia Molecular, Universidade Federal de Santa Maria, Santa Maria RS Brazil

[*] Corresponding author: E-mail: laura.orian@unipd.it

Abstract

Methylmercury is a highly toxic compound and human exposure is mainly related to consumption of polluted fish and seafood. The inactivation of thiol-based enzymes, promoted by the strong affinity binding of electrophilic mercuric ions to thiol and selenol groups of proteins, is likely an important factor explaining its toxicity. A key role is played by the chemistry and reactivity of the mercury-chalcogens bond, particularly Hg-S and Hg-Se, which is the focus of this computational work (level of theory: (COSMO)-ZORA-BLYP-D3(BJ)/TZ2P). We analyze nine ligand-exchange model reactions (the so-called Rabenstein's reactions) involving an entering ligand (methylchalcogenolate) and a substrate (methylchalcogenolatemethylmercury). Trends in reaction and activation energies are discussed and a change in mechanism is reported for all cases when going from gas-phase to water, that is from a single-well PES to a canonical S_N2-like mechanism. The reasons accounting for the biochemically challenging and desired displacement of methylmercury from a seleno/thiol protein can be found already in these model reactions, as can be seen from the similarities of the ligand exchange reactions in solution in thermodynamics and kinetics.

Introduction

Methylmercury (CH_3Hg^+), the methylated form of mercury, is a hazardous neurotoxicant, naturally found in the environment and in food chain.[1,2] Several studies have demonstrated that the CH_3Hg^+ toxicity might involve its interaction with thio- and selenoproteins (due to the high affinity of mercury to sulfur and selenium atoms present in cysteine (Cys) and selenocysteine (Sec) residues, respectively), disrupting their normal function.[3,4]

CH_3Hg^+ might bind to the Cys residue in many proteins and peptides, such as thioredoxin (Trx) and glutathione (GSH), which are the Thioredoxin Reductase (TrxR) and Glutathione

Peroxidase (GPx) substrates, leading to the decrease in the active concentration of these important substrates. In addition, the adducts between Trx and GSH with CH_3Hg^+ (Trx-$HgCH_3$ and GS-$HgCH_3$) might deliver the CH_3Hg^+ moiety to its respective enzymes, inhibiting them.[5,6] As a consequence of these exchange reactions, CH_3Hg^+ can be distributed easily in the organism, according to the Rabenstein's reaction (Eq. 1).

$$RS(e)H + R'S(e)HgCH_3 \rightleftarrows R'S(e)H + RS(e)HgCH_3 \quad (1)$$

The adducts between CH_3Hg^+ and Cys residues are highly stable. However, the S-Hg bond is labile, and in the presence of another thiol (-SH) or selenol (-SeH) groups, exchange reactions may occur. Furthermore, the formation of R-Se-$HgCH_3$ complexes is more favorable than R-S-$HgCH_3$, due to the higher binding affinity between CH_3Hg^+ and –SeH.[4,7–10]

The GPx and TrxR are important selenoenzymes involved in the cell antioxidant defense, cell proliferation, and redox-regulated signaling cascades. GPx is able to reduce hydrogen peroxide and/or organic hydroperoxides to water and/or the corresponding alcohols, respectively,[11,12] while the TrxR can reduce many substrates, such as the oxidized thioredoxin, peroxides, and other disulfide proteins (Scheme 1A and B).[13,14] It is supposed that the GPx and TrxR inhibition by CH_3Hg^+ occurs via the binding of CH_3Hg^+ to the selenium atom of Sec in their active site, leading to the interruption of the catalytic cycle (Scheme 1C and D), and consequently increasing the reactive oxygen species (ROS) levels, causing cell death.[4,15]

However, CH_3Hg^+ mechanism of action is still not well understood and computational methods have been applied to gain insight into methylmercury chemistry with cysteine and selenocysteine. Particularly, Schreckenbach and co-workers carried out an extensive analysis on structural, electronic and thermodynamic properties of methylmercury complexes with cysteine and selenocysteine, but also on the chalcogenophilicity of mercury, assessing that Hg-S bond has a higher bond dissociation energy (BDE) than Hg-Se and Hg-Te in different compounds ranging from small molecules to large complexes. In addition, they investigated *in silico* the thermodynamic feasibility of a degradation mechanism of selenocysteinate complexes of methylmercury[16–20] in order to rationalize mercury-selenium antagonism.[21] The development of an accurate computational method to study CH_3Hg^+ binding, interactions, and reactivity is critical for future work focused on model compounds as well as on systems of increasing complexity up to the thiol- and selenol-based enzymes.

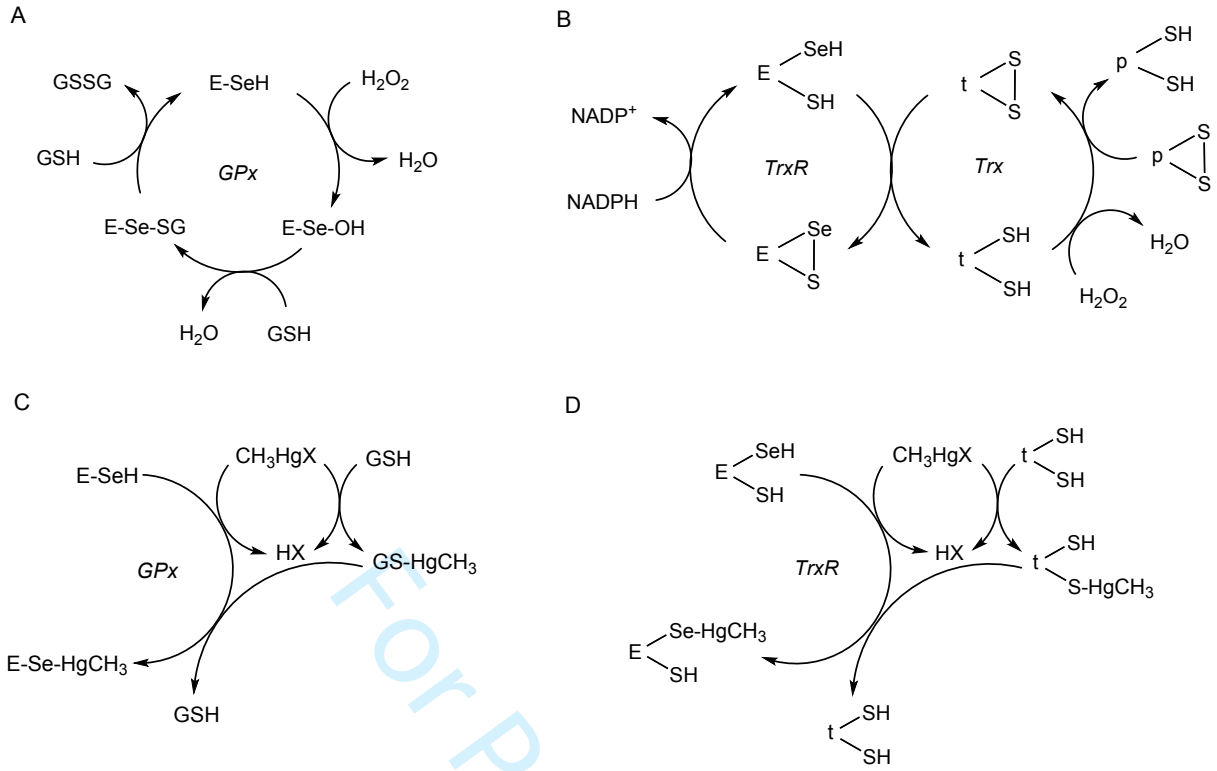

Scheme 1. Catalytic cycle of GPx (A) and TrxR (B) enzymes, and their inhibition by MeHg (C and D, respectively). The enzymes inhibition may occur after the binding of MeHg to the Se atom in Sec residue. E, t, p, and X represent the enzyme, Trx, other disulfide proteins, and chloride/hydroxide anion.

In this work, we have analyzed the reaction of a methylchalcogenolate and a methylchalcogenolatemethylmercury substrate, which affords the formation of a new dinuclear substrate and cleavage of the methylchalcogenolate initially bonded to mercury. These model systems represent the situation in which mercury is bonded to a Cys or a Sec in an enzymatic pocket with the presence of a thiol like glutathione; alternatively, they represent methylmercury bonded to a free cysteine entering in an enzymatic pocket and binding to the active Cys or Sec present in the site. Suitable DFT computational methodologies for structural as well as energetic investigation are discussed and the reaction mechanisms are studied in gas phase as well as in water.

Methods

All Density Functional Theory (DFT) calculations were done with the Amsterdam Density Functional (ADF) program.[22,23] Zeroth-order regular approximation (ZORA) was used in order to include scalar relativistic effects due to the presence of heavy nuclei.[24] Four different functionals were tested, i.e. two GGA (OLYP[25–27], BLYP[26,28]), one hybrid (B3LYP[26,29,30]) and one meta-hybrid (M06-2X[31,32]). In addition, the effect of including Grimme dispersion[33–36] was investigated for BLYP and

B3LYP (BLYP-D3(BJ) and B3LYP-D3(BJ)). The TZ2P basis set, a large uncontracted set of Slater-type orbitals (STOs) of triple-ζ quality, augmented with two sets of polarization functions on each atom was used for every atom. Frozen core approximation was not used in the benchmark calculations, to allow a rigorous comparison among all the chosen functionals (small frozen-core approximation is not available for B3LYP and M06-2X in ADF); in these cases, the all electron basis set is denoted TZ2P-ae. Frequency calculations were performed for all fully optimized geometries. All minima have real frequencies, and all transition states have one imaginary frequency corresponding to the correct normal mode connecting reactants to products. Enthalpies and Gibbs free energies at 298.15 K and 1 atm (ΔG) were calculated from electronic bond energies (ΔE) and our frequency computations using standard statistical-mechanics relationships for an ideal gas, and are reported in Supporting information (Tables S7-S9). Since the trends are identical, in the text we discuss electronic bond energies (ΔE).

For a representative set of reactions, an intrinsic reaction coordinate (IRC) calculation was performed to obtain the reaction profile. The IRC profile is the steepest-descent path from the saddle point (the transition state) to the local minima, representing the reactants and products for the investigated reaction.[37] In these calculations, solvation effects (water) were taken into account using the conductor-like screening model (COSMO)[38], as implemented in ADF. For water, we used an effective radius of 1.93Å for the solvent-excluding surface, derived from the macroscopic density, 78.39 as the relative dielectric constants and the molecular mass. We chose as 0.00 the empirical parameter in the scaling function in the COSMO equation. We used MM3 radii[39] divided by 1.2.

In order to ascertain the correctness of the implicit solvation, analyses were also carried out with an explicit solvent model. The extended tight-binding semi-empirical program GFNn-xTB by Grimme et al.[40,41] was used to build a network of water molecules and subsequently to reoptimize some critical structures with the explicit solvation.

To gain quantitative insight into the stability of a representative set of compounds, we performed activation strain (ASA) and energy decomposition analysis (EDA)[42–44] as implemented in ADF. Using this fragment based approach, according to the ASA scheme, we have decomposed the energy relative to the reactants into *strain*, ΔE_{strain} (i.e. the deformation energy required by the reactants to acquire the structure they have in the compound of interest) and *interaction,* ΔE_{int} *(i.e.* the interaction energy between the deformed reactants) (Eq. 2):

$$\Delta E = \Delta E_{strain} + \Delta E_{int} \quad (2)$$

Within EDA, ΔE_{int} can be written as the sum of *electrostatic interaction* (ΔV_{elstat}), the interaction between Coulomb charge densities, *Pauli repulsion* (ΔE_{Pauli}), related to the repulsive interaction between filled orbitals, *orbital interaction* (ΔE_{oi}) due to stabilizing interactions such as HOMO-LUMO interaction, and *dispersion* (ΔE_{disp}), which takes into account dispersive interactions (Eq. 3):

$$\Delta E_{int} = \Delta V_{elstat} + \Delta E_{Pauli} + \Delta E_{oi} + \Delta E_{disp} \quad (3)$$

To assess the quality of the employed functionals, reference energies were obtained also using the single-reference multiconfiguration domain-based local pair natural orbital coupled cluster singles doubles perturbative triples (DLPNO-CCSD(T)) method, [45] implemented as part of the ORCA computational suite [46,47] . All electron relativistic contracted basis set aug-cc-pVTZ-DK with Douglas−Kroll−Hess (DKH) scalar relativistic Hamiltonians [48] were used.[49]

Results and discussion

The focus of this work is the reaction between a methylchalcogenolate and a methylchalcogenolatemethylmercury substrate in gas phase (GP) and in water (Scheme 2). This ligand-exchange reaction was chosen as a simplified model of the so-called Rabenstein's reaction, involved in the absorption, distribution and excretion of methylmercury from the human body.[4,10] The reaction might proceed either with the formation of a stable three-centers intermediate bismethylchalcogenolatemethylmercurate (TCI) or with a S_N2-like mechanism. These mechanisms closely resemble the reaction between a methylchalcogenolate and a dimethyldichalcogenide, thoroughly investigated by some of us.[50]

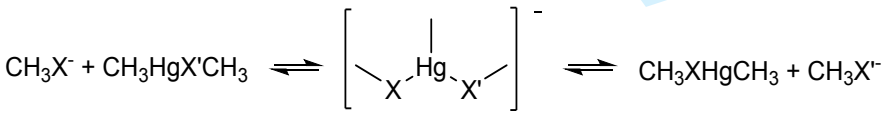

Scheme 2. Model Rabenstein's reaction; X, X' = S, Se, Te.

For clarity, we labelled every compound by the chalcogen(s) and mercury it contains, including the net charge but excluding the methyl groups, i.e. CH_3-S^- is denoted as **S**$^-$, CH_3-Hg-S-CH_3 is **Hg-S**, the three-centers intermediate is **S-Hg-S**$^-$ and so on.

First, we present our benchmark results, carried out on the reaction **S**$^-$ + **Hg-S** in gas-phase: for this reaction, a stable three-center intermediate was easily located at all the tested levels of theory. We focus a) on the different conformers of **S-Hg-S**$^-$; b) on the energetics for the formation of **S-Hg-S**$^-$ described with the different functionals and c) on the relevant geometrical parameters of **Hg-S**. Then,

we extend our investigation to the same reaction including selenium and tellurium. Finally, the results of mechanistic calculations in water are reported and discussed. The effect of the chalcogen and of the solvent were investigated for the influence on both thermodynamics and reaction mechanism

S-Hg-S$^-$ conformers

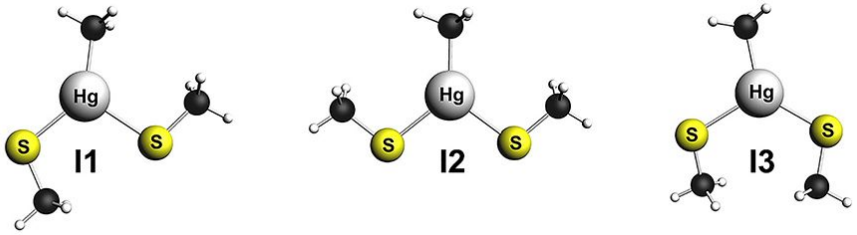

Figure 1. Fully optimized structures of **S-Hg-S**$^-$ denoted isomers **I1**, **I2** and **I3**; level of theory: ZORA-OLYP/TZ2P.

With all the tested functionals, we obtained three conformers for **S-Hg-S**$^-$, as previously reported with cysteinate instead of methylthiolate.[20] Their fully optimized structures are shown in Figure 1, while the energies computed at different levels of theory are reported in Table 1. As a reference, the energies were also calculated at DKH-DLPNO-CCSD(T)/aug-cc-pVTZ-DK level of theory using the OLYP fully optimized structure of each conformer. Since it is well known that geometry is less sensitive to functional/basis sets, we chose OLYP optimization results for our CCSD(T) calculations. In addition, this functional has been benchmarked for organochalcogenides[51] and, by using the same level of theory, it is possible to immediately compare reactivity properties in absence and in presence of methylmercury.

Table 1. Energies (kcal mol^{-1}) relative to the most stable conformer computed with the tested functionals combined with TZ2P-ae basis set for all the atoms; CCSD(T) single point calculations were done using ZORA-OLYP/TZ2P fully optimized geometries. Energy values obtained with small-core TZ2P basis sets, when available, are reported in parentheses.

	OLYP	BLYP	BLYP-D3(BJ)	B3LYP	B3LYP-D3(BJ)	M06-2X	CCSD(T)
I1	0.00 (0.00)	0.00 (0.00)	0.00 (0.00)	0.00	0.00	0.00	0.00
I2	0.98 (0.92)	1.26 (1.24)	2.50 (2.47)	1.56	2.61	3.20	1.82
I3	1.51 (1.49)	1.38 (1.39)	1.01 (1.07)	1.53	1.30	1.14	2.45

In all cases, the conformer **I1** is the most stable one. In general, the relative stability of **I2** and **I3** changes from functional to functional. In agreement with the CCSD(T) trend, pure GGA functionals (OLYP and BLYP) predict **I3** to be the least stable conformer; conversely, the hybrid, the meta-hybrid

and in general the dispersion corrected functionals predict **I2** to be the least stable one. However, BLYP and B3LYP values are definitively too close to establish a meaningful distinction between the stability of **I2** and **I3**. Because, in all cases, the differences in energy between the conformers are within a few kcal mol^{-1}, we chose to retain for further investigation only **I2** conformers, whose intrinsic symmetry reduces the number of structures to calculate when different chalcogens are present on the substrate and on the nucleophile.

A conformational analysis on similar three-center complexes has been done using Stuttgart-Dresden basis set[52] for Hg at B3LYP/SDD (Hg), 6-311+G(p) (S, Se), 6-31+G(p) (H, C, N, O) level of theory by Asaduzzaman et al. with a whole cysteinate/selenocysteinate instead of methylchalcogenolate as nucleophile. A different stability trend was found, i.e. **I2** was identified as the most stable conformer.[20]

Formation energy of S-Hg-S^-

Focusing on **I2**, we computed the formation energies of this **S-Hg-S^-** conformer with all the functionals included in our benchmark (Table 2). At all tested levels of theory, ΔE for the formation of the **S-Hg-S^-** from the free reactants is strongly negative, suggesting highly thermodynamic feasibility. The least and the largest negative values are found with OLYP and B3LYP-D3(BJ), respectively. As expected, the inclusion of dispersion leads to larger (more negative) ΔE values, as can be seen when comparing BLYP vs BLYP-D3(BJ) and B3LYP vs B3LYP-D3(BJ) results. The best agreement with the CCSD(T) value is obtained at ZORA-BLYP-D3(BJ)/TZ2P level of theory. Energies calculated with small-core approximation in the basis set combined to every functional but B3LYP and M06-2X show the same trend and, even in these cases, BLYP-D3(BJ) is the functional affording better agreement with the highly correlated *ab initio* calculations. Gibbs free energies and reaction enthalpies follow the same trend of electronic energies. (Table S7).

Table 2. Formation energies (ΔE) of **S-Hg-S**$^-$ computed with the tested functionals combined with TZ2P-ae basis set for all the atoms and absolute deviations (ΔΔE) of the formation energies (kcal mol^{-1}) with respect to CCSD(T) single point calculations done using ZORA-OLYP/TZ2P fully optimized geometry (ΔE =-27.89). Values obtained with small-core approximation basis set, when available, are reported in parentheses. The investigated reaction is: S^- + Hg-S ⇄ S-Hg-S^-.

Functional	ΔE	ΔΔE
OLYP	-19.49 (-19.04)	8.40 (9.95)
BLYP	-22.93 (-22.60)	4.96 (5.29)
BLYP-D3(BJ)	-28.06 (-27.76)	-0.17 (0.13)
B3LYP	-23.94	3.95
B3LYP-D3(BJ)	-28.48	-0.59
M06-2X	-28.09	-0.20

Structural parameters

The validation of the computed molecular geometries was assessed comparing relevant interatomic distances and angles of the substrate **Hg-S** and MCYSHG10 (Scheme 3) to crystallographic data of similar compounds extracted from the Cambridge Structural Database(CSD).[53] Results are reported in Table 3 and Table 4, respectively.

Table 3. Relevant interatomic distances and angles of **Hg-S** compared to available crystallographic structures (Scheme 3).

	Bond length (Å)			Angles and dihedrals (º)		
	S–Hg	Hg–C	C–S	S–Hg–C	C–S–Hg	C–S–Hg–C
OLYP	2.38	2.11	1.84	178	103	180
BLYP	2.40	2.14	1.86	178	103	180
BLYP-D3(BJ)	2.40	2.14	1.86	179	102	179
B3LYP	2.38	2.12	1.84	178	103	180
B3LYP-D3(BJ)	2.37	2.12	1.84	179	102	179
M06-2X	2.36	2.09	1.83	179	102	180
x-ray (CSD)						
MCYSHG10[a]	2.35	2.10	1.81	178	100	110
PENMHG10[b]	2.38	2.06	1.86	175	107	130
FADVAI[c]	2.35	2.07	1.81	176	100	175

[a] Data taken from Taylor et al. [54]; [b] Data taken from Wong et al[55]; [c] Data taken from Belakhov et al. [56]

Table 4. Relevant interatomic distances and angles computed for MCYSHG10 compared to the crystallographic structure. (Scheme 3)

	Bond length (Å)			Angles and dihedrals (°)		
	S–Hg	Hg–C	C–S	S–Hg–C	C–S–Hg	C–S–Hg–C
OLYP	2.38	2.11	1.84	177	106	159
BLYP	2.41	2.14	1.87	177	105	161
BLYP-D3(BJ)	2.41	2.14	1.86	178	103	176
B3LYP	2.39	2.11	1.84	177	105	163
B3LYP-D3(BJ)	2.38	2.11	1.84	178	104	177
M06-2X	2.37	2.09	1.83	178	103	179
x-ray (CSD)						
MCYSHG10[a]	2.35	2.10	1.81	178	100	110

[a] Data taken from Taylor et al. [54]

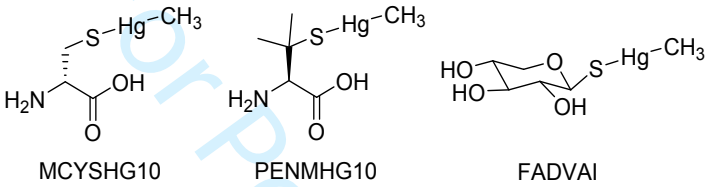

Scheme 3. Mono coordinated methylmercury complexes taken from CSD for structural comparison purposes (Tables 3 and 4)

No structural data exist for our simple methylated structures, so we compared the relevant geometrical parameters of **Hg-S** those of mono coordinated methylmercury complexes sketched in Scheme 3. For **Hg-S**, there is a good agreement between all the calculated and the experimental bond lengths and angles, with little to almost no differences in the parameters computed at different levels of theory. Discrepancies between experimental and *in silico* parameters are of a few hundredths of Å for bond lengths and of a few degrees for angles.

In order to make a more precise comparison between calculated and crystallographic parameters, we chose to optimize the structure of MCYSHG10 (Scheme 3) at all six levels of theory investigated for **Hg-S**. The relevant geometric parameters are reported in Table 4. As precedently stated comparing **Hg-S** computed parameters to the experimental parameters of the compounds in Scheme 3, little to almost no difference is found when using the different levels of theories and all the values are close to the experimental ones. All differences are within a few hundredths of Å for bond lengths and a few degrees for angles. Only C-S-Hg-C dihedral differs from the crystallographic one, likely because of packing effect.

Based on the benchmark results, considering energy and structural results, BLYP-D3(BJ) combined with TZ2P basis sets for all the atoms was chosen for our systematic investigation on model Rabenstein's reactions. M06-2X also performed well in the prediction of both energy values and

structural parameters but was excluded since is computationally more demanding than the dispersion-corrected GGA.

Results obtained with the cheap OLYP functional are also considered to assess the error when tackling these systems with a pure GGA functional. Both OLYP and BLYP-D3(BJ) have been employed successfully for mechanistic studies involving methyl- and aryl-chalcogenides.[50,57–59]

Mechanism of the Rabenstein's reactions

The gas-phase mechanism of the Rabenstein's reactions was investigated changing S, Se, Te on the entering ligand and on the substrate; overall nine reactions were considered. The results are shown in Table 5.

Table 5. Electronic energies (ΔE) relative to reactants (kcal mol^{-1}) of the stationary points in gas-phase computed at three different levels of theory, i.e. ZORA-OLYP/TZ2P, ZORA-BLYP-D3(BJ)/TZ2P and CCSD(T) single point calculations, which were done using ZORA-OLYP/TZ2P fully optimized geometries.

	OLYP		**BLYP-D3(BJ)**		**CCSD(T)**	
	TCI	P	TCI	P	TCI	P
S$^-$+Hg-S	-19.04	0.00	-27.76	0.00	-27.89	0.00
S$^-$+Hg-Se	-20.53	-2.71	-29.35	-2.64	-29.64	-2.71
S$^-$+Hg-Te	-23.22	-8.69	-31.97	-8.11	-32.48	-8.66
Se$^-$+Hg-S	-17.82	2.71	-26.71	2.64	-26.93	2.71
Se$^-$+Hg-Se	- 19.26	0.00	-28.16	0.00	-28.64	0.00
Se$^-$+Hg-Te	- 21.93	-5.98	-30.76	-5.47	-31.46	-5.95
Te$^-$+Hg-S	-14.53	8.69	-23.86	8.11	-23.82	8.66
Te$^-$+Hg-Se	-15.95	5.98	-25.29	5.47	-25.51	5.95
Te$^-$+Hg-Te	-18.48	0.00	-27.80	0.00	-28.23	0.00

We chose to compare the trends obtained with OLYP functional, which well described the energetics for the reaction of a methylchalcogenolate and a dimethyldichalcogenide substrate[50] and BLYP-D3(BJ), which best reproduced the CCSD(T) results in the case of **S$^-$+Hg-S**. At ZORA-OLYP/TZ2P level, all the reactions proceed via a single-well mechanism without any appreciable barrier for the formation of a three-center intermediate (TCI) from the reactants and from the TCI to the products. This is in agreement with typical S_N2 reactions involving heavy central atoms.[60] The inclusion of dispersion (BLYP-D3(BJ)) leads to slightly asymmetric TCIs even when two equal chalcogenolates are bonded to the methylmercury moiety. By analogy with the trichalcogenides[50], this suggests the

existence of two equivalent structures near the bottom of the potential energy surface, separated by a low-energy transition state. Thus, the reaction energy profile is likely a flattened double well curve, but the complete characterization of these low-energy transition states and the exploration of the whole potential energy surface around TCI weren't pursued since they would not provide additional useful information on the reaction. In all cases, the TCI is highly stabilized with respect to the free reactants. As in the model **S**$^-$ +**Hg-S** reaction used in the benchmark, ZORA-BLYP-D3(BJ)/TZ2P results nicely agree with CCSD(T) calculations performed on OLYP fully optimized geometries also when changing the chalcogen from S, to Se and Te in the entering ligand as well as in the substrate. Importantly, ZORA-OLYP/TZ2P values show the same trend, but their high deviation from the *ab initio* results for the TCIs formation energy lead us to consider in the discussion mainly the energetics computed with the dispersion corrected functional.

From the data of Table 5, the effect of changing chalcogen in the entering ligand can be seen. Particularly, when going from **S**$^-$, to **Se**$^-$ and to **Te**$^-$, the TCIs become progressively less stable and the effect is more remarkable when passing from Se to Te. This is likely due to the stabilization of the negative charge, which becomes more diffuse on the entering ligand when increasing the size of the chalcogen, weakening the electrostatic contribution to the formation of the TCI. The same trend is observed for the overall reaction energy, which becomes less and less negative when going from S$^-$ to Se$^-$ and Te$^-$. Comparing the entering ligand and the leaving methylchalcogenolate it can be seen that the stabilization of the negative charge which, in gas phase, is energetically favored on the heavier chalcogens plays a key role in establishing the trend in these processes. The trends in thermodynamics, in fact, are those expected considering nucleophilicity and leaving group capabilities in gas phase. Particularly, the energetics of the reactions changes significantly, since **S**$^-$ + **Hg-X** is favored in all cases while **Te**$^-$ +**Hg-X** is unfavored in all cases. An intermediate situation is found with the **Hg-Se** substrate: the reaction with **S**$^-$ has a negative ΔE, while the reaction with **Te**$^-$ has a positive ΔE. The presence of a different chalcogen in the substrate leads to a stabilization of the TCIs, which increases by approximately 2 kcal mol^{-1} when going from **Hg-S** to **Hg-Se** and **Hg-Te**. Also, the overall reaction becomes more favorable for the same entering ligand when a substrate with a heavier chalcogen is involved. The explanation based on charge distribution effects nicely fits these results too, since in the TCIs/products the charge is more diffuse when a heavier chalcogen is present/cleaved on/from the substrate, leading to larger stabilization. Gibbs free energies obtained at both levels of theory show the same trends. (Table S8).

Notably, all these trends do not depend on the level of theory and, for what concerns the overall reaction energy trends, there is a good agreement between all the three tested methods. Even if OLYP,

the cheapest functional used in this work, leads to significantly underestimated (about 10 kcal mol^{-1}) TCI formation energies, it correctly predicts trends in agreement with more sophisticated computational approaches.

Table 6. ASA and EDA (kcal mol^{-1}) of the TCIs at ZORA-BLYP-D3(BJ)/TZ2P. The fragments are **S$^-$** and **Hg-X**.

	S-Hg-S$^-$	**S-Hg-Se$^-$**	**S-Hg-Te$^-$**
ΔE	-27.76	-29.35	-31.97
ΔE_{strain}	28.97	27.54	25.42
ΔE_{int}	-56.73	-56.89	-57.39
ΔE_{elstat}	-122.47	-123.45	-124.58
ΔE_{Pauli}	129.80	132.09	134.73
ΔE_{oi}	-59.22	-60.58	-62.43
ΔE_{disp}	-4.84	-4.95	-5.11

In order to obtain a quantitative insight into the TCI stability with respect to the free reactants we performed ASA and EDA according to Eqs. 2 and 3, choosing **S$^-$** and **Hg-X** as fragments, i.e. focusing on the formation energies of **S-Hg-S$^-$**, **S-Hg-Se$^-$**, **S-Hg-Te$^-$** with respect to different substrates (**Hg-S**, **Hg-Se**, **Hg-Te**), and the results are shown in Table 6 and Figure S1.

For the attack of S$^-$ to HgX, little to almost no difference is present in the interaction energy, which remains almost constant for the three intermediates. The formation energy of the three-center intermediate becomes more negative when increasing the size of the chalcogen on the substrate principally because of a net decrease of the strain energy when going from **Hg-S** to **Hg-Se** to **Hg-Te**, because the bonds become more and more soft. The stability of the TCI with respect to different substrates appears to be *strain-controlled*, while the changes in electrostatic interaction, Pauli repulsion and orbital interaction compensate each other leading to no significant change to the overall interaction energy. Also, dispersion variations play a marginal role and do not vary appreciably.

We extended our investigation on the model Rabenstein's reactions carrying out mechanistic calculations in water. Again, both ZORA-OLYP/TZ2P and ZORA-BLYP-D3(BJ)/TZ2P were used and the results are shown in Table 7. Gibbs free energies follow essentially the same behavior (Table S9).

Table 7. Electronic energies (ΔE) relative to reactants (kcal mol^{-1}) of the stationary points in water computed at two different levels of theory, i.e. COSMO-ZORA-OLYP/TZ2P and COSMO-ZORA-BLYP-D3(BJ)/TZ2P. Activation energies relative to reactant complexes (RC), when present, are shown in parentheses. PC refers to product complexes.

	OLYP			BLYP-D3(BJ)		
	TS	P	RC	TS	PC	P
S^-+Hg-S	4.27	0.00	-7.01	-5.23(1.78)	-7.01	0.00
S^-+Hg-Se	3.93	0.56	-7.17	-5.66(1.51)	-7.20	0.62
S^-+Hg-Te	3.50	1.47	-7.43	-5.96(1.47)	-6.86	2.19
Se^-+Hg-S	3.37	-0.56	-7.82	-6.28(1.54)	-7.79	-0.62
Se^-+Hg-Se	3.00	0.00	-8.00	-6.76(1.24)	-8.00	0.00
Se^-+Hg-Te	2.54	0.91	-8.33	-7.10(1.23)	-7.77	1.58
Te^-+Hg-S	2.03	-1.47	-9.05	-8.15(0.90)	-9.62	-2.19
Te^-+Hg-Se	1.63	-0.91	-9.35	-8.68(0.67)	-9.91	-1.58
Te^-+Hg-Te	1.10	0.00	-9.73	-9.13(0.60)	-9.73	0.00

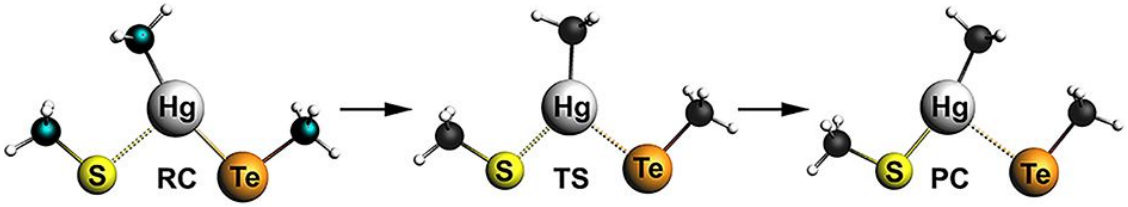

Figure 2. Fully optimized structures of reactant complex (RC), transition state (TS) and product complex (PC) for the reaction **S^-+Hg-Te**, computed at COSMO-ZORA-BLYP-D3(BJ)/TZ2P level of theory.

Moving from gas-phase to solvent, both functionals predict a change in mechanism. While in gas-phase the reaction proceeds with a single-well profile, in water at COSMO-ZORA-OLYP/TZ2P level of theory, a unimodal potential energy surface is found, suggesting a S_N2-like mechanism (Figure S2). The three-center species identified as a minimum on the PES in gas-phase, converged as transition states at higher energy with respect to the free reactants in water.

No stable three-center intermediates were located even when adding dispersion at COSMO-ZORA-BLYP-D3(BJ)/TZ2P. In this latter case, the reaction profile is a true double-well with a transition state at negative energies with respect to the free reactants, connecting weakly bonded reactant complexes to product complexes, both stabilized with respect to the free reactants and products (Figure 2) The shift downward of the BLYP-D3(BJ) PES with respect to the OLYP PES suggests also at this level of theory a S_N2-like mechanism. (Figure 3)

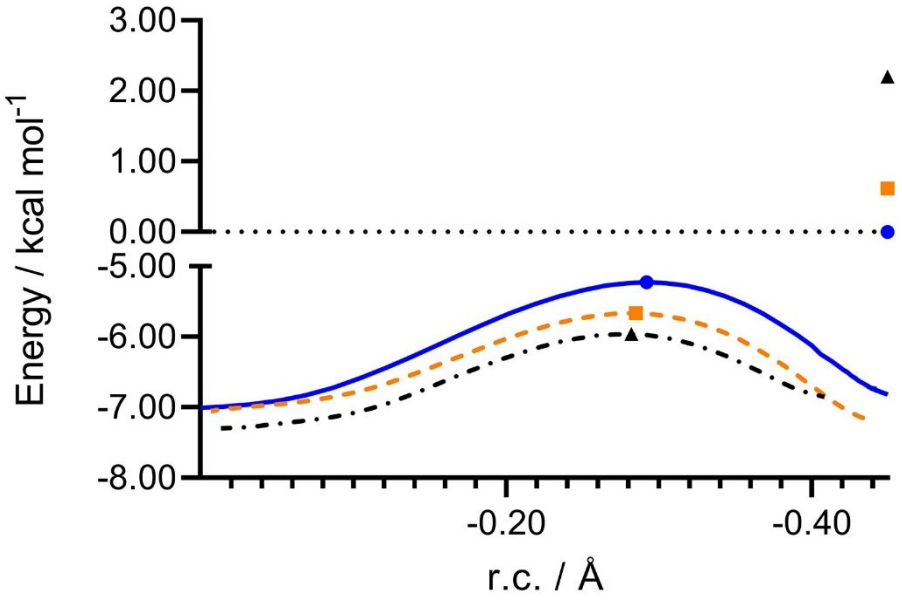

Figure 3. Reaction profiles for **S**$^-$+**Hg-X** (X=S (blue solid line), Se (orange dashed line), Te (black dash-dotted line)) in water, computed at COSMO-ZORA-BLYP-D3(BJ)/TZ2P. The reaction coordinate (r.c.) is defined as r.c. = (d_{Hg-S} - d_{Hg-S}^0), where d_{Hg-S}^0 refers to the Hg-S bond length in the reactant complex of each reaction. Filled dots (X=S (circles), Se (squares), Te (triangles)) represent the position of the transition states and the energy value of the free products for each reaction. Since the product complexes are much more stabilized than the free products, the energy axis has been cut and the free products appear on the upper right corner of the graph.

Both OLYP and BLYP-D3(BJ) predict an inversion in the overall reaction thermodynamic trends, with respect to the gas phase. This is in agreement with the known concept of polar solvent stabilizing better species where the charge is more localized.[61,62] The destabilization of the three-center intermediate, where the charge is more diffuse compared to the free reactants, is strong enough to turn the stable gas phase TCI into a transition state.

Changing the chalcogen on the entering ligand from S, to Se and to Te leads to progressively stabilized products. This can make the ligand exchange reaction turn from unfavored (**S**$^-$ + **Hg-Se**) to favored (**Te**$^-$ + **Hg-Se**) with implications in methylmercury biochemistry. Conversely, changing the chalcogen on the substrate from S, to Se and to Te leads to an increase of the reaction energy, which becomes more positive as the chalcogen becomes heavier. A similar inversion in the thermodynamic trends was theoretically investigated by Riccardi et al. who observed that in gas-phase Hg^{2+} prefers hard ligands, while in water the expected HSAB theory trend is recovered, with Hg^{2+} preferring softer ligands.[63]

All the activation energies computed at COSMO-ZORA/BLYP-D3(BJ)/TZ2P are below 2 kcal mol^{-1}, and the differences between them are too small to establish some meaningful distinction, particularly when S and Se are involved. All the values are close to those computed for **S**$^-$ + **Hg-S**,

which has been experimentally described, with different thiolates, as an almost diffusion-controlled associative ligand exchange reaction. [8]

The TCIs have also been optimized in explicit solvent without finding substantial differences from the continuum solvation description. After creating a box of water molecules, the TCIs have been inserted and the system has been optimized without any potential or geometrical constraints. As obtained with the COSMO model, the system evolves to a natural Hg-X bond disruption (see Supporting information).

Conclusions

In this work, we have employed a scalar relativistic DFT approach to analyze ligand-exchange model reactions, known as Rabenstein's reactions, involving an entering ligand (methylchalcogenolate) and a substrate (methylchalcogenolatemethylmercury). The major outcome of our preliminary benchmark, carried out including the zeroth order regular approximation (ZORA) for the relativistic effects and Slater type all electron basis sets of triple-ζ quality with two polarization functions (TZ2P ae), is that BLYP-D3(BJ), that is the method we recommend for these and analogous molecular systems, performs rather well in describing the relevant structural features as well as the energetics. Another functional which provides results in nice agreement with crystallographic structures and CCSD(T) calculations is M06-2X. Importantly, the pure GGA OLYP works well for geometry optimizations, and, despite energies show deviations of almost 10 kcal mol^{-1} from CCSD(T) reference values, it reproduces correctly the trends observed when changing the chalcogens.

The reaction profile in gas phase shows a single minimum, which corresponds to a stable three-center intermediate (TCI). The stability of the TCI increases with increasing chalcogen size in the substrate and decreases when increasing the chalcogen size in the entering ligand. The extent of charge diffusion explains these trends and the trend in the overall reaction energy which becomes less and less negative when going from $\mathbf{S^-}$ to $\mathbf{Se^-}$ and $\mathbf{Te^-}$. Notably, it emerges that $\mathbf{S^-}$ + **Hg-X** is favored in all cases while $\mathbf{Te^-}$ +**Hg-X** is unfavored in all cases; when the substrate is **Hg-Se**, the reaction with $\mathbf{S^-}$ has a negative ΔE, while the reaction with $\mathbf{Te^-}$ has a positive ΔE.

When modeling the Rabenstein's reactions in water, using COSMO continuum description of the condensed phase, a change in mechanism is observed in all cases. The profiles computed at COSMO-ZORA/BLYP-D3(BJ)/TZ2P are characterized by the presence of reactant and product complexes, stabilized with respect to the free reactants and products, respectively, connected by a transition state.

The change in mechanism from gas to condensed phase is analogous to those reported for S_N2 reactions[60] at P[64], or at X (X=S, Se),[50] and is here described for a ligand exchange reaction at Hg. The profiles involving methylthiolate as entering ligand, which are the most interesting from a biochemical point of view, show that **S**$^-$ + **Hg-S** and **S**$^-$ + **Hg-Se** have rather similar energetics, characterized by low activation and neutral reaction energies. In a hydrophobic environment, such as an enzymatic cavity where water is not allowed into, an intermediate regime between the gas phase and the water mechanism is expected, as extensively investigated for reactions with a similar behavior.[64] For the specific case of **S**$^-$ + **Hg-Se**, the products lay at -0.14 kcal mol^{-1} with respect to the free reactants, showing an almost neutral, even if slightly favorite, reaction energy. (Table S6) We must stress that substituents and weak interactions inside the enzymatic cavity may play an important role in tuning the displacement of methylmercury bonded to a selenoprotein by a thiolate. This analysis paves the way for mechanistic investigations of methylmercury bonding to thiol- and seleno-targets of increasing complexity, with the ambitious goal of understanding its toxicology *in silico* and rationally designing paths of detoxification.

Conflict of interest

There are no conflicts to declare.

Acknowledgements

This research was funded by the Università degli Studi di Padova, thanks to the P-DiSC (BIRD2018-UNIPD) project MAD^{3}S (Modeling Antioxidant Drugs: Design and Development of computer-aided molecular Systems); P.I. L.O. All the calculations were carried out on Galileo (CINECA: Casalecchio di Reno, Italy) thanks to the ISCRA Grant MEMES (MEthylMErcury and Selenoproteins), P.I.: L.O. M.D.T. is grateful to Fondazione CARIPARO forfinancial support (PhD grant). J.R., O.F., and P.N. would like to thank the financial support by Coordination for Improvement of Higher Education Personnel CAPES/PROEX (n° 23038.005848/2018-31; n°0737/2018; n°88882.182123/2018-01; nº 88887.354370/2019-00), the CAPES/PrInt – Institutional Internationalization Project (nº 88887.374997/2019-00), the National Council for Scientific and Technological Development (CNPq), and the Rio Grande do Sul Foundation for Research Support (FAPERGS). The authors are grateful to the anonymous referees for their insightful suggestions, which have contributed to improve the quality of this work.

References

[1] M. R. Karagas, A. L. Choi, E. Oken, M. Horvat, R. Schoeny, E. Kamai, W. Cowell, P. Grandjean, S. Korrick, *Environ. Health Perspect.* **2012**, *120*, 799–806.

[2] Y. S. Hong, Y. M. Kim, K. E. Lee, *J. Prev. Med. Public Heal.* **2012**, *45*, 353–363.

[3] J. L. Franco, T. Posser, P. R. Dunkley, P. W. Dickson, J. J. Mattos, R. Martins, A. C. D. Bainy, M. R. Marques, A. L. Dafre, M. Farina, *Free Radic. Biol. Med.* **2009**, *47*, 449–457.

[4] P. A. Nogara, C. S. Oliveira, G. L. Schmitz, P. C. Piquini, M. Farina, M. Aschner, J. B. T. Rocha, *Biochim. Biophys. Acta - Gen. Subj.* **2019**, *1863*, 129284.

[5] V. Branco, C. Carvalho, *Biochim. Biophys. Acta - Gen. Subj.* **2019**, *1863*, 129255.

[6] M. Farina, M. Aschner, *Biochim. Biophys. Acta - Gen. Subj.* **2019**, *1863*, 129285.

[7] D. L. Rabenstein, C. A. Evans, *Bioinorg. Chem.* **1978**, *8*, 107–114.

[8] D. L. Rabenstein, R. S. Reid, *Inorg. Chem.* **1984**, *23*, 1246–1250.

[9] D. L. Rabenstein, *J. Chem. Educ.* **1978**, *55*, 292–296.

[10] A. P. Arnold, K. S. Tan, D. L. Rabenstein, *Inorg. Chem.* **1986**, *25*, 2433–2437.

[11] M. Bortoli, M. Torsello, F. M. Bickelhaupt, L. Orian, *ChemPhysChem* **2017**, *18*, 2990–2998.

[12] L. Orian, P. Mauri, A. Roveri, S. Toppo, L. Benazzi, V. Bosello-Travain, A. De Palma, M. Maiorino, G. Miotto, M. Zaccarin, et al., *Free Radic. Biol. Med.* **2015**, *87*, 1–14.

[13] R. B. Flohé, M. Maiorino, *Biochim. Biophys. Acta - Gen. Subj.* **2013**, *1830*, 3289–3303.

[14] E. S. J. Arnér, *Biochim. Biophys. Acta - Gen. Subj.* **2009**, *1790*, 495–526.

[15] H. Steinbrenner, H. Sies, *Biochim. Biophys. Acta - Gen. Subj.* **2009**, *1790*, 1478–1485.

[16] J. M. Parks, J. C. Smith, *Methods in Enzymology*, Elsevier Inc., **2016**, p 103-122

[17] A. M. Asaduzzaman, M. A. K. Khan, G. Schreckenbach, F. Wang, *Inorg. Chem.* **2010**, *49*, 870–878.

[18] A. Asaduzzaman, D. Riccardi, A. T. Afaneh, S. J. Cooper, J. C. Smith, F. Wang, J. M. Parks, G. Schreckenbach, *Acc. Chem. Res.* **2019**, *52*, 379–388.

[19] A. M. Asaduzzaman, G. Schreckenbach, *Inorg. Chem.* **2011**, *50*, 3791–3798.

[20] A. M. Asaduzzaman, G. Schreckenbach, *Inorg. Chem.* **2011**, *50*, 2366–2372.

[21] M. A. K. Khan, F. Wang, *Environ. Toxicol. Chem.* **2009**, *28*, 1567–1577.

[22] G. te Velde, F. M. Bickelhaupt, E. J. Baerends, C. Fonseca Guerra, S. J. A. van Gisbergen, J. G. Snijders, T. Ziegler, *J. Comput. Chem.* **2001**, *22*, 931–967.

[23] E. J. Baerends, T. Ziegler, A. J. Atkins, J. Autschbach, D. Bashford, O. Baseggio, A. Bérces, F. M. Bickelhaupt, C. Bo, P. M. Boerritger, L. Cavallo, C. Daul, D. P. Chong, D. V Chulhai, L. Deng, R. M. Dickson, J. M. Dieterich, D. E. Ellis, M. van Faassen, A. Ghysels, A. Giammona, S. J. A. van Gisbergen, A. Goez, A. W. Götz, S. Gusarov, F. E. Harris, P. van den Hoek, Z. Hu, C. R. Jacob, H. Jacobsen, L. Jensen, L. Joubert, J. W. Kaminski, G. van Kessel, C. König, F. Kootstra, A. Kovalenko, M. Krykunov, E. van Lenthe, D. A. McCormack, A. Michalak, M. Mitoraj, S. M. Morton, J. Neugebauer, V. P. Nicu, L. Noodleman, V. P. Osinga, S. Patchkovskii, M. Pavanello, C. A. Peeples, P. H. T. Philipsen, D. Post, C. C. Pye, H. Ramanantoanina, P. Ramos, W. Ravenek, J. I. Rodríguez, P. Ros, R. Rüger, P. R. T. Schipper, D. Schlüns, H. van Schoot, G. Schreckenbach, J. S. Seldenthuis, M. Seth, J. G. Snijders, M. Solà, S. M., M. Swart, D. Swerhone, G. te Velde, V. Tognetti, P. Vernooijs, L. Versluis, L. Visscher, O. Visser, F. Wang, T. A. Wesolowski, E. M. van Wezenbeek, G. Wiesenekker, S. K. Wolff, T. K. Woo and A. L. Yakovlev, ADF2018, SCM, Theoretical Chemistry, Vrije Universiteit, Amsterdam, The Netherlands.

[24] E. Van Lenthe, E. J. Baerends, J. G. Snijders, *J. Chem. Phys.* **1994**, *101*, 9783–9792.

[25] N. C. Handy, A. J. Cohen, *Mol. Phys.* **2001**, *99*, 403–412.

[26] C. Lee, W. Yang, R. G. Parr, *Phys. Rev. B* **1988**, *37*, 785–789.

[27] B. G. Johnson, P. M. W. Gill, J. A. Pople, *J. Chem. Phys.* **1993**, *98*, 5612–5626.

[28] A. D. Becke, *Phys. Rev. A* **1988**, *38*, 3098–3100.

[29] A. D. Becke, *J. Chem. Phys.* **1993**, *98*, 5648–5652.

[30] P. J. Stephens, F. J. Devlin, C. F. Chabalowski, M. J. Frisch, *J. Phys. Chem.* **1994**, *98*, 11623–11627.

[31] Y. Zhao, D. G. Truhlar, *Theor. Chem. Acc.* **2008**, *120*, 215–241.

[32] Y. Zhao, D. G. Truhlar, *J. Chem. Phys.* **2006**, *125*, 194101.

[33] S. Grimme, S. Ehrlich, L. Goerigk, *J. Comput. Chem.* **2011**, *32*, 1456–1465.

[34] A. D. Becke, E. R. Johnson, *J. Chem. Phys.* **2005**, *123*, 154101.

[35] E. R. Johnson, A. D. Becke, *J. Chem. Phys.* **2005**, *123*, 024101.

[36] A. D. Becke, E. R. Johnson, *J. Chem. Phys.* **2005**, *122*, 154104.

[37] L. Deng, T. Ziegler, *Int. J. Quantum Chem.* **1994**, *52*, 731–765.

[38] A. Klamt, G. Schüürmann, *J. Chem. Soc. Perkin Trans. 2* **1993**, 799–805.

[39] N. L. Allinger, X. Zhou, J. Bergsma, *J. Mol. Struct. THEOCHEM* **1994**, *312*, 69–83.

[40] S. Grimme, C. Bannwarth, P. Shushkov, *J. Chem. Theory Comput.* **2017**, *13*, 1989–2009.

[41] C. Bannwarth, S. Ehlert, S. Grimme, *J. Chem. Theory Comput.* **2019**, *15*, 1652–1671.

[42] F. M. Bickelhaupt, E. J. Baerends, *Rev. Comput. Chem.* **2000**, *15*, 1–86.

[43] F. M. Bickelhaupt, K. N. Houk, *Angew. Chemie - Int. Ed.* **2017**, *56*, 10070–10086.

[44] T. Ziegler, A. Rauk, *Inorg. Chem.* **1979**, *18*, 1558–1565.

[45] D. G. Liakos, Y. Guo, F. Neese, *J. Phys. Chem. A* **2020**, *124*, 90–100.

[46] F. Neese, *Wiley Interdiscip. Rev. Comput. Mol. Sci.* **2012**, *2*, 73–78.

[47] F. Neese, *Wiley Interdiscip. Rev. Comput. Mol. Sci.* **2018**, *8*, e1327

[48] F. Neese, A. Wolf, T. Fleig, M. Reiher, B. A. Hess, *J. Chem. Phys.* **2005**, *122*, 204107

[49] D. A. Pantazis, F. Neese, *Wiley Interdiscip. Rev. Comput. Mol. Sci.* **2014**, *4*, 363–374.

[50] M. Bortoli, L. P. Wolters, L. Orian, F. M. Bickelhaupt, *J. Chem. Theory Comput.* **2016**, *12*, 2752–2761.

[51] F. Zaccaria, L. P. Wolters, C. Fonseca Guerra, L. Orian, *J. Comput. Chem.* **2016**, *37*, 1672–1680.

[52] D. Figgen, G. Rauhat, M. Dolg, H. Stoll, *Chem. Phys.* **2005**, *311*, 227.

[53] C. R. Groom, I. J. Bruno, M. P. Lightfoot, S. C. Ward, *Acta Crystallogr. Sect. B Struct. Sci. Cryst. Eng. Mater.* **2016**, *72*, 171–179.

[54] N. . Taylor, Y. S. Wong, P. C. Chieh, A. J. Carty, *J.C.S. Dalt. Trans* **1975**, *5*, 438–442.

[55] Y. S. Wong, A. J. Carty, C. Chieh, *J.C.S. Dalt. Trans* **1977**, *19*, 1801–1808.

[56] V. Belakhov, E. Dor, J. Hershenhorn, M. Botoshansky, T. Bravman, M. Kolog, Y. Shoham, G. Shoham, T. Baasov, *Isr. J. Chem.* **2000**, *40*, 177–188.

[57] M. Bortoli, F. Zaccaria, M. D. Tiezza, M. Bruschi, C. F. Guerra, F. Matthias Bickelhaupt, L. Orian, *Phys. Chem. Chem. Phys.* **2018**, *20*, 20874–20885.

[58] M. Bortoli, S. M. Ahmad, T. A. Hamlin, F. M. Bickelhaupt, L. Orian, *Phys. Chem. Chem. Phys.* **2018**, *20*, 27592–27599.

[59] M. Bortoli, M. Bruschi, M. Swart, L. Orian, *New J. Chem.* **2020**, *44*, 6724-6731

[60] T. A. Hamlin, M. Swart, F. M. Bickelhaupt, *ChemPhysChem* **2018**, *19*, 1315–1330.

[61] J. K. Laerdahl, E. Uggerud, *Int. J. Mass Spectrom.* **2002**, *214*, 277–314.

[62] G. Schreckenbach, *Chem. - A Eur. J.* **2017**, *23*, 3797–3803.

[63] D. Riccardi, H. B. Guo, J. M. Parks, B. Gu, A. O. Summers, S. M. Miller, L. Liang, J. C. Smith, *J. Phys. Chem. Lett.* **2013**, *4*, 2317–2322.

[64] T. A. Hamlin, B. van Beek, L. P. Wolters, F. M. Bickelhaupt, *Chem. - A Eur. J.* **2018**, *24*, 5927–5938.

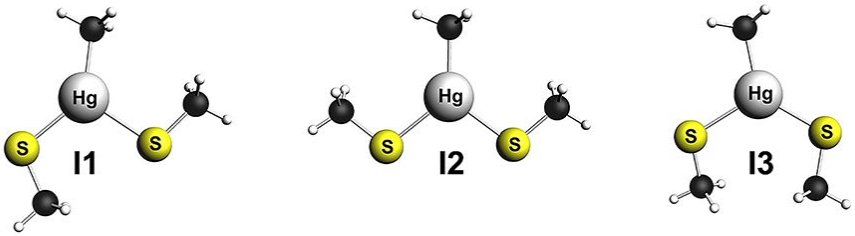

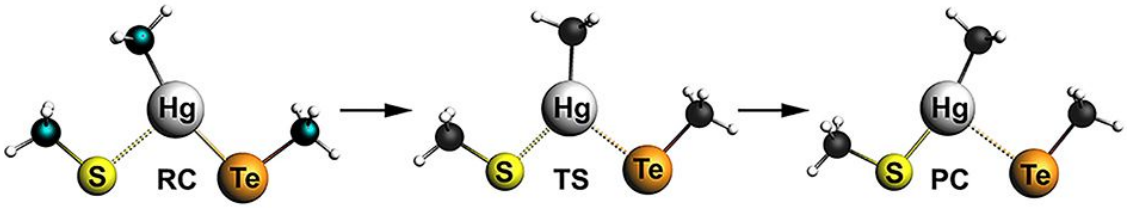

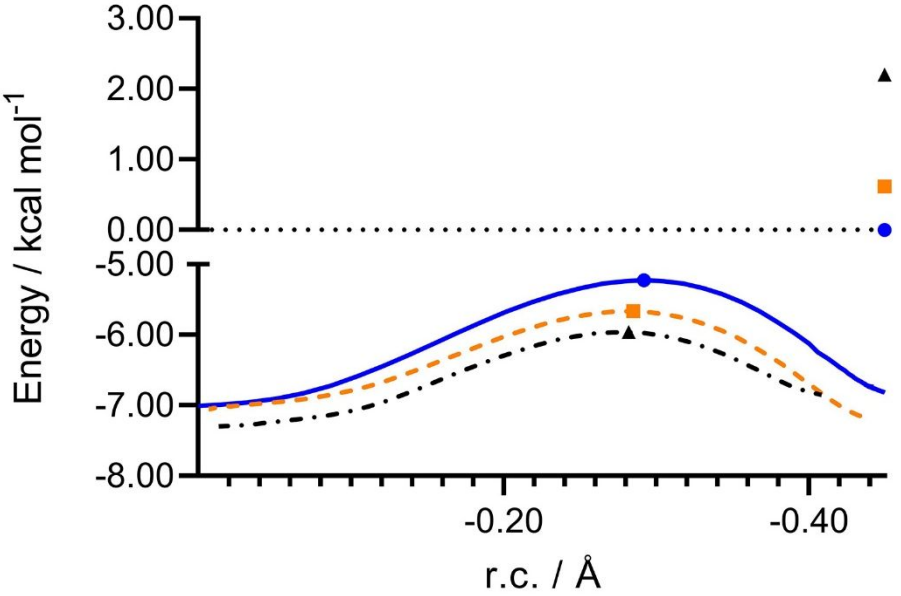

Table 1. Energies (kcal mol^{-1}) relative to the most stable conformer computed with the tested functionals combined with TZ2P-ae basis set for all the atoms; CCSD(T) single point calculations were done using ZORA-OLYP/TZ2P fully optimized geometries. Energy values obtained with small-core TZ2P basis sets, when available, are reported in parentheses.

	OLYP	**BLYP**	**BLYP-D3(BJ)**	**B3LYP**	**B3LYP-D3(BJ)**	**M06-2X**	**CCSD(T)**
I1	0.00 (0.00)	0.00 (0.00)	0.00 (0.00)	0.00	0.00	0.00	0.00
I2	0.98 (0.92)	1.26 (1.24)	2.50 (2.47)	1.56	2.61	3.20	1.82
I3	1.51 (1.49)	1.38 (1.39)	1.01 (1.07)	1.53	1.30	1.14	2.45

Table 2. Formation energies (ΔE) of **S-Hg-S**$^-$ computed with the tested functionals combined with TZ2P-ae basis set for all the atoms and absolute deviations (ΔΔE) of the formation energies (kcal mol^{-1}) with respect to CCSD(T) single point calculations done using ZORA-OLYP/TZ2P fully optimized geometry (ΔE =-27.89). Values obtained with small-core approximation basis set, when available, are reported in parentheses. The investigated reaction is: S^- + Hg-S ⇄ S-Hg-S^-.

Functional	ΔE	ΔΔE
OLYP	-19.49 (-19.04)	8.40 (9.95)
BLYP	-22.93 (-22.60)	4.96 (5.29)
BLYP-D3(BJ)	-28.06 (-27.76)	-0.17 (0.13)
B3LYP	-23.94	3.95
B3LYP-D3(BJ)	-28.48	-0.59
M06-2X	-28.09	-0.20

Table 3. Relevant interatomic distances and angles of **Hg-S** compared to available crystallographic structures (Scheme 3).

	Bond length (Å)			Angles and dihedrals (º)		
	S–Hg	Hg–C	C–S	S–Hg–C	C–S–Hg	C–S–Hg–C
OLYP	2.38	2.11	1.84	178	103	180
BLYP	2.40	2.14	1.86	178	103	180
BLYP-D3(BJ)	2.40	2.14	1.86	179	102	179
B3LYP	2.38	2.12	1.84	178	103	180
B3LYP-D3(BJ)	2.37	2.12	1.84	179	102	179
M06-2X	2.36	2.09	1.83	179	102	180
x-ray (CSD)						
MCYSHG10[a]	2.35	2.10	1.81	178	100	110
PENMHG10[b]	2.38	2.06	1.86	175	107	130
FADVAI[c]	2.35	2.07	1.81	176	100	175

[a] Data taken from Taylor et al. [54]; [b] Data taken from Wong et al[55]; [c] Data taken from Belakhov et al. [56]

Table 4. Relevant interatomic distances and angles computed for MCYSHG10 compared to the crystallographic structure. (Scheme 3)

	Bond length (Å)			Angles and dihedrals (º)		
	S–Hg	Hg–C	C–S	S–Hg–C	C–S–Hg	C–S–Hg–C
OLYP	2.38	2.11	1.84	177	106	159
BLYP	2.41	2.14	1.87	177	105	161
BLYP-D3(BJ)	2.41	2.14	1.86	178	103	176
B3LYP	2.39	2.11	1.84	177	105	163
B3LYP-D3(BJ)	2.38	2.11	1.84	178	104	177
M06-2X	2.37	2.09	1.83	178	103	179
x-ray (CSD)						
MCYSHG10[a]	2.35	2.10	1.81	178	100	110

[a] Data taken from Taylor et al. [54]

Table 5. Electronic energies (ΔE) relative to reactants (kcal mol^{-1}) of the stationary points in gas-phase computed at three different levels of theory, i.e. ZORA-OLYP/TZ2P, ZORA-BLYP-D3(BJ)/TZ2P and CCSD(T) single point calculations, which were done using ZORA-OLYP/TZ2P fully optimized geometries.

	OLYP		**BLYP-D3(BJ)**		**CCSD(T)**	
	TCI	P	TCI	P	TCI	P
S^-+Hg-S	-19.04	0.00	-27.76	0.00	-27.89	0.00
S^-+Hg-Se	-20.53	-2.71	-29.35	-2.64	-29.64	-2.71
S^-+Hg-Te	-23.22	-8.69	-31.97	-8.11	-32.48	-8.66
Se^-+Hg-S	-17.82	2.71	-26.71	2.64	-26.93	2.71
Se^-+Hg-Se	- 19.26	0.00	-28.16	0.00	-28.64	0.00
Se^-+Hg-Te	- 21.93	-5.98	-30.76	-5.47	-31.46	-5.95
Te^-+Hg-S	-14.53	8.69	-23.86	8.11	-23.82	8.66
Te^-+Hg-Se	-15.95	5.98	-25.29	5.47	-25.51	5.95
Te^-+Hg-Te	-18.48	0.00	-27.80	0.00	-28.23	0.00

Table 6. ASA and EDA (kcal mol^{-1}) of the TCIs at ZORA-BLYP-D3(BJ)/TZ2P. The fragments are **S$^-$** and **Hg-X**.

	S-Hg-S$^-$	**S-Hg-Se$^-$**	**S-Hg-Te$^-$**
ΔE	-27.76	-29.35	-31.97
ΔE_{strain}	28.97	27.54	25.42
ΔE_{int}	-56.73	-56.89	-57.39
ΔE_{elstat}	-122.47	-123.45	-124.58
ΔE_{Pauli}	129.80	132.09	134.73
ΔE_{oi}	-59.22	-60.58	-62.43
ΔE_{disp}	-4.84	-4.95	-5.11